



Analysis of climate and landscape change through the Pennsylvanian and Permian Monongahela and Dunkard Groups, Southeastern Ohio, USA

Daniel I. Hembree¹ · Connor J. McFadden¹

Received: 4 June 2020 / Revised: 7 July 2020 / Accepted: 15 July 2020 / Published online: 24 July 2020
© Springer Nature Switzerland AG 2020

Abstract

Paleosols and ichnofossils of the Late Pennsylvanian to Early Permian Monongahela and Dunkard groups of southeastern Ohio provide significant paleoenvironmental and paleoclimatic data related to the Late Paleozoic climatic transition. Forty paleosol profiles from three outcrops in southeastern Ohio were investigated. Methods included the description of paleosol profiles in the field and the analysis of thin sections. Clay mineralogy and bulk geochemistry were used to assess weathering processes and paleoprecipitation. Results, such as the distribution, abundance, and size of physical features including slickensides, pedogenic carbonates, and rhizoliths suggest erratic fluctuations between mildly seasonal wet environments and strongly seasonal dry environments throughout the studied section which are supported by oscillations in calculated paleoprecipitation values. Paleosols of the Monongahela Group are interpreted as mildly to strongly seasonal, wet to wet-dry, sparsely to heavily vegetated fen, dry woodland, clastic marsh, early successional vegetation, and brakeland ecosystems forming on proximal to distal floodplain and shoreline lacustrine environments. Paleosols of the Lower Dunkard Group are interpreted as a mildly to strongly seasonal, wet to wet-dry, sparsely to heavily vegetated, clastic marsh, early successional vegetation, and brakeland ecosystems forming on proximal to distal floodplain and distal levee environments. Variability in climate has profound effects on paleolandscapes. By investigating changes in paleosols through episodes of climatic transition, we can better understand the impact these changes have on soils and soil ecosystems of the past and future.

Keywords Paleosols · Ichnofossils · Continental · Paleoenvironment · Paleoecology

1 Introduction

Soils are dynamic, open systems which form the foundation of terrestrial ecosystems (Buol et al. 2003). They are vital in storing atmospheric gases, regulating and partitioning water flow, filtering contaminants, and hosting an extensive reservoir of biodiversity (Lavelle and Spain 2001; Buol et al. 2003). The physical and chemical properties of soils

are directly influenced by their environment of formation allowing paleosols to provide significant paleoenvironmental and paleoecological information at local and regional scales (Kraus 1999; Retallack 2001; Buol et al. 2003). Therefore, the study of paleosols is critical to our understanding of Earth and life processes throughout geologic time.

This study involved the investigation of short-term climate variability and related changes in terrestrial paleolandscapes of the Appalachian Basin during the Late Paleozoic climate transition through the study of paleosols and ichnofossils of the Monongahela and Lower Dunkard groups in southeastern Ohio. The Upper Pennsylvanian to Lower Permian Monongahela and Dunkard groups consist of fluvial and lacustrine sediments deposited during a transition from a largely wet-seasonal to dry-seasonal climate (Driese and Ober 2005; King 2008; Fedorko and Skema 2013; Montañez and Cecil 2013; Hembree and Carnes 2018). Several studies conducted in the western United States have utilized paleosols to investigate the Late Paleozoic climatic transition

Communicated by M. V. Alves Martins

Electronic supplementary material The online version of this article (<https://doi.org/10.1007/s43217-020-00022-7>) contains supplementary material, which is available to authorized users.

✉ Daniel I. Hembree
hembree@ohio.edu

¹ Department of Geological Sciences, Ohio University, 316 Clippinger Laboratories, Athens, OH 45701, USA

(Kessler et al. 2001; Tabor and Montañez 2004; DiMichele et al. 2006; Mack et al. 2010; Giles et al. 2013; Counts and Hasiotis 2014; Tanner and Lucas 2017), however, far fewer studies have focused on paleosols of this interval in the Appalachian Basin. In this study, paleosols spanning the Late Pennsylvanian to Early Permian boundary provided a detailed understanding of spatial and temporal changes in soil environments, landscape evolution, and paleoclimate during this critical time in Earth history.

2 Geologic setting

2.1 Late Pennsylvanian to Early Permian climatic transition

During the Late Pennsylvanian to Early Permian significant changes were occurring in the Earth system making it a critical time for study. The continents Laurussia and Gondwana were in their final phases of tectonic collision (Tabor and Poulsen 2008). This collision led to the uplift of the east–west oriented Central Pangaean mountain chain and plateau (Blakey 2008; Tabor and Poulsen 2008). During this episode of tectonic activity, two major glaciations occurred with the orogenic uplands acting as nucleation centers for ice sheets (Gastaldo et al. 1996; Fielding et al. 2008; Montañez and Poulsen 2013). From the Mississippian to the Middle Pennsylvanian ice sheets advanced in western Gondwana (South America) (Gastaldo et al. 1996; Fielding et al. 2008). This was followed by an interglacial period until the Early Permian ending with the growth of ice sheets in eastern Gondwana (Australia) (Gastaldo et al. 1996; Fielding et al. 2008). Intervals of glaciation and deglaciation had a significant effect on global atmospheric circulation patterns (Gastaldo et al. 1996; Cecil et al. 2003; Tabor and Poulsen 2008). During glacial intervals, atmospheric high pressure zones existed over Gondwanan ice sheets causing the contraction of the intertropical convergence zone (ITCZ) towards the equator and its movement over a narrower latitudinal range (Gastaldo et al. 1996; Cecil et al. 2003; Tabor and Poulsen 2008). This resulted in maximum compression of the doldrums belt suppressing seasonal excursions and producing a more ever-wet, stable climate in the equatorial region from the Mississippian to the Middle Pennsylvanian (Gastaldo et al. 1996; Cecil et al. 2003; Tabor and Poulsen 2008). During interglacials, polar high pressure cells were minimized causing an expansion of the ITCZ over a wider latitudinal belt (Gastaldo et al. 1996; Cecil et al. 2003; Tabor and Poulsen 2008). This resulted in a wider distribution of the doldrums producing a comparably drier, more seasonal climate in the equatorial region during the Late Pennsylvanian to Early Permian (Gastaldo et al. 1996; Cecil et al. 2003; Tabor and Poulsen 2008; Cecil 2013).

2.2 Monongahela and Dunkard groups

The Monongahela and Dunkard groups were deposited within the central to northern Appalachian Basin located to the west of the ancestral Appalachians, close to the equator (Montañez and Cecil 2013). Climatic drying was likely enhanced within the basin by its position in the continental interior, isolating it from moist air currents (Cecil 2013). The Monongahela and Dunkard groups are predominantly composed of fluvial and lacustrine sediments deposited on an upper to lower fluvial plain (Martin 1998; King 2008; Hembree and Bowen 2017). The Monongahela Group is considered Gzhelian in age and is regionally divided into the Pittsburgh and Uniontown formations (Fig. 1a) (Martin 1998). It is represented by shale, mudstone, sandstone, and limestone which crop out in Ohio, West Virginia, and Pennsylvania (Sturgeon 1958; King 2008; Fedorko and Skema 2013). The Dunkard Group is regionally divided into the Waynesburg, Washington, and Greene formations (Fig. 1b) (Martin 1998; Fedorko and Skema 2013). It is represented by shale, siltstone, mudstone, sandstone, limestone and coal (Martin 1998; Fedorko and Skema 2013). The age of this group has been debated due to limited biostratigraphic control (pollen and plants) (Clendening 1972; Martin 1998; Eble et al. 2013). Recent use of insect and vertebrate biostratigraphy as well as freshwater bivalves has strengthened the argument for a Permian age of the entire unit (Martin 1998; Lucas 2013; Schneider et al. 2013).

2.3 Late Pennsylvanian to Early Permian paleosols

Studies of paleosols of the Appalachian Basin and the midcontinent of the United States have shown a transition from Upper Pennsylvanian paleosols with redox features, little to no carbonate nodules, and little to no vertic features to Lower Permian paleosols with oxidizing features, abundant carbonate nodules, and prominent vertic features. Hembree and Bowen's (2017) study of Upper Monongahela and Lower Dunkard group paleosols yielded an upward trend of decreasing mean annual precipitation (MAP) and increasing seasonality. This same transition was recognized by Hembree and Carnes (2018) in three Upper Monongahela and Lower Dunkard group outcrops. A third study conducted by Hembree and Blair (2016) on outcrops of the Washington Formation revealed thick, repeating successions of calcareous Vertisols characteristic of dry and seasonal conditions. Studies of paleosols of this age from the midcontinent of the United States had produced a similar pattern. Studies conducted by Tabor and Montañez (2004) and DiMichele et al. (2006) in the Wichita, Bowie, and Pease River groups as well as the

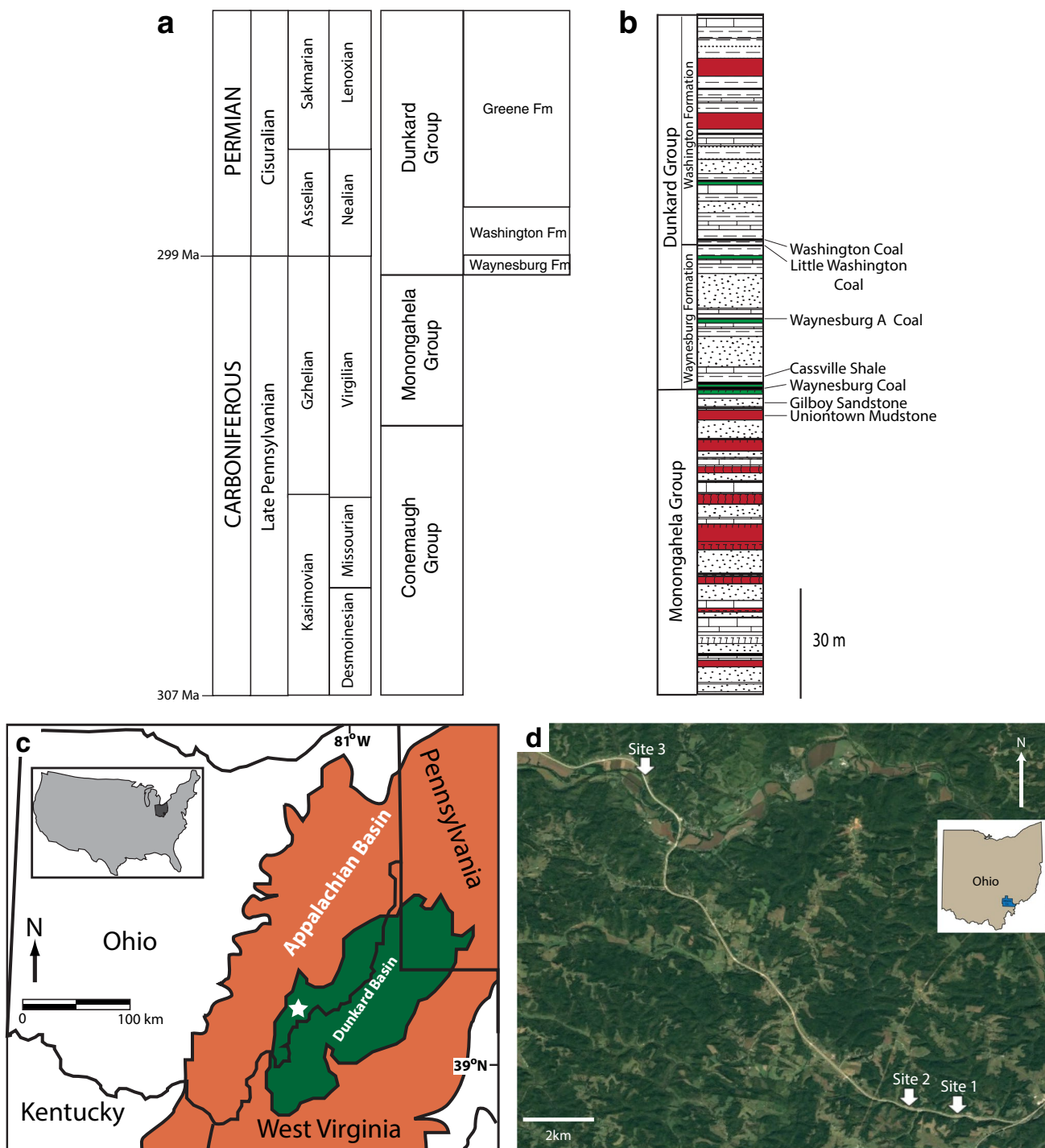


Fig. 1 **a** General stratigraphic column displaying the geologic age and time periods of the Conemaugh, Monongahela, and Dunkard groups. **b** General lithologic stratigraphic column of Upper Monongahela and Lower Dunkard groups (Sturgeon 1958; Fedorko and Skema 2013; Hembree and Bowen 2017) highlighting known paleosol units as well as identifiable marker beds. **c** Location of the study area (at

star) within Ohio (blue) relative to the Appalachian (orange) and Dunkard (green) basins (from Hembree and Bowen 2017). Inset map show the position of Ohio within the United States. **d** Aerial image of the study area (sites 1–3) along US Route 50, Athens County, Ohio (highlighted in inset map of Ohio)

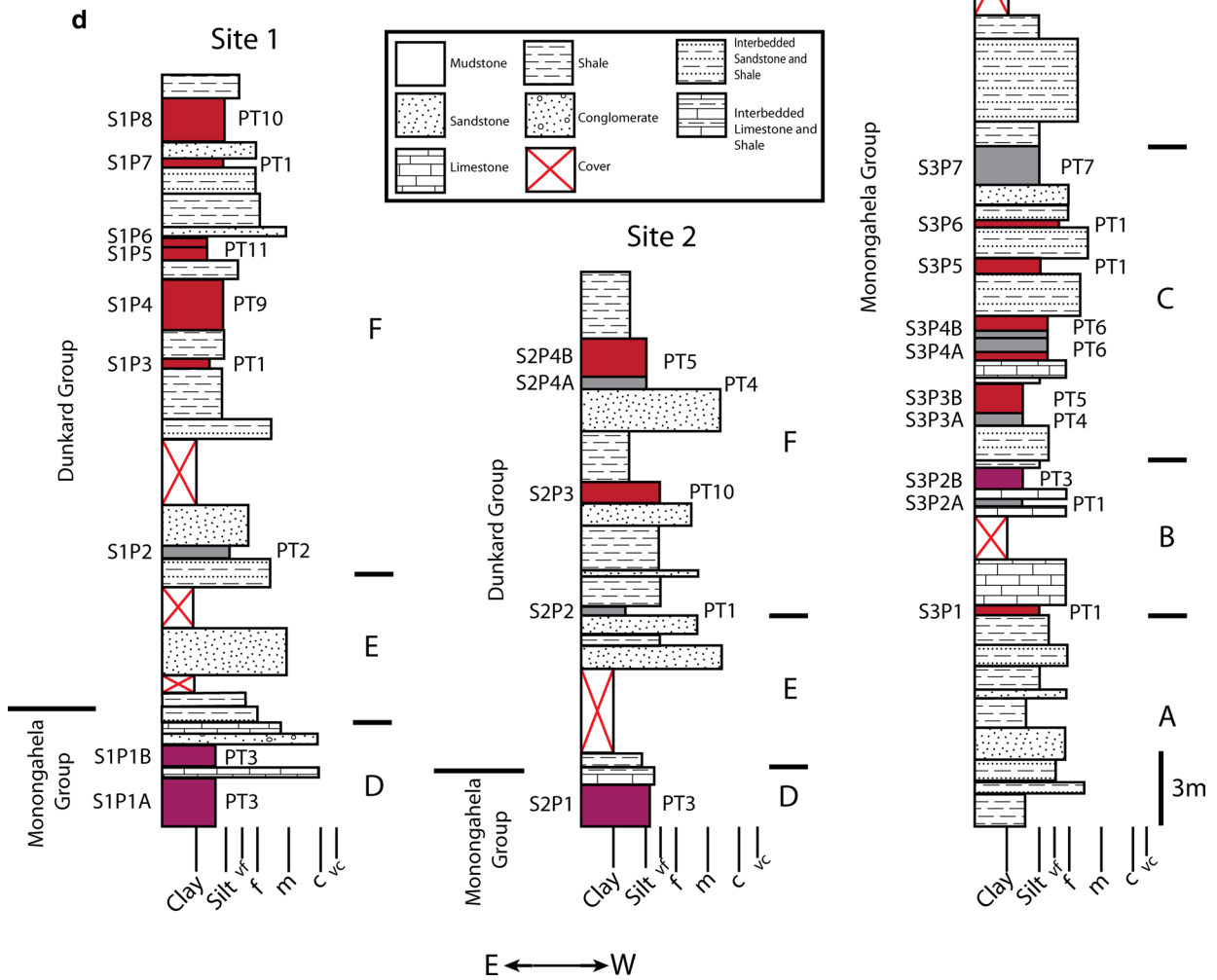


Fig. 2 Outcrops and general sections of sites 1–3. **a** Site 1 (39° 12' 47.73" N, 81° 49' 59.93" W) is 30 m high and includes the upper Monongahela and lower Dunkard groups. **b** Site 2 (39° 12' 51.67" N, 81° 50' 52.58" W) is 22 m high and includes the upper Monongahela and lower Dunkard groups. **c** Site 3 (39° 18' 14.00" N, 81° 56' 19.80" W) is 55 m high includes the upper Conemaugh and Monongahela groups. Red lines indicate approximate locations of described paleosols and lithologies. **d** General stratigraphic columns documenting contacts of the Monongahela and Dunkard groups, major lithologies, paleosol sections, and pedotypes

Lueders and Clear Fork formations of Texas revealed an upward shift from waterlogged floodplain paleosols (Histosols, Ultisols) in the Upper Pennsylvanian to well-drained paleosols (Alfisols, Aridisols, Calcic Vertisols) in the Lower Permian. Paleosols of the Lower Permian Abo and Sangre de Cristo formations suggested a semi-arid to sub-humid seasonal climate based on vertic features, calcareous nodules, and root traces (Mack et al. 2003; Tanner and Lucas 2017). The Lower Permian Wellington Formation of Oklahoma contains similar paleosols as well as evaporate layers strengthening the interpretation of seasonal conditions (Giles et al. 2013). Paleosol cores described from the Lower Permian Council Grove Group of Kansas were indicative of a semi-arid, but moist, environment (Counts and Hasiotis 2014). A similar study of Lower Permian cores in northeastern New Mexico identified dolomitic Protosols and Dolosols indicating seasonality and aridity (Kessler et al. 2001). These studies generally support a temporal trend of drying and increasing seasonality. However, the details of this transition and effects on landscapes at finer scales did vary between the different basins.

3 Methodology

3.1 Field methods

The study area consisted of three, 22-to-55 m thick outcrops (Sites 1–3) beginning approximately 2.5 km southwest of Coolville, (Athens County), Ohio, USA and extending 13 km northwest along US Route 50 ending roughly 14 km east of Athens, Ohio, USA (Fig. 1c, d). One general stratigraphic section was constructed at each site documenting major lithologies and identifying paleosols (Fig. 2). Paleosols identified within each section were excavated in 1–2 m wide and 50 cm deep trenches; physical properties such as contacts, color, texture, structure, horizons, and ichnofossils were described every 20–40 vertical cm and detailed sections were produced for each paleosol. Ichnofossils including rhizoliths were described. Samples for laboratory analysis were collected down the paleosol sections every 20–40 vertical cm. For each paleosol section, one to four samples

were collected for thin section analysis, one to five for X-ray fluorescence (XRF), and one for X-ray diffraction (XRD).

3.2 Laboratory methods

A total of 54 thin sections (44 1.0×2.0 cm, 9 1.5×3.0 cm, 1 2.0×3.0 cm slides) were prepared by Texas Petrographic (Houston, Texas) and then examined and photographed using a Motic BA300 polarizing microscope and Moticam 10-megapixel camera, respectively. Grain size, microstructure, microfabric, mineralogy, root traces and channels, burrows, organic matter, Fe–Mn oxides, and carbonate content were described for each thin section.

Bulk geochemistry of 75 paleosol samples was determined by ALS Minerals (Reno, Nevada) through X-ray fluorescence (XRF) to determine the weight percent of major oxides (SiO₂, TiO₂, Al₂O₃, Fe₂O₃, CaO, MgO, Na₂O, K₂O) (Electronic Supplemetry Material Appendix A). This process consisted of the analysis of dried and homogenized, 0.7 g samples through lithium borate fusion XRF. Samples were prepared using the fusion-bead method with a lithium metaborate flux. Analysis was conducted with a XRF spectrometer PANalytical, model Axios Fast. The resulting data was reported as weight percentages of each major oxide and then normalized to molecular weights. These data were used to calculate various molecular weathering ratios (Retallack 2001; Sheldon and Tabor 2009) (Table 1). The mole fraction of oxides obtained from XRF data were also used to calculate the chemical index of alteration minus potassium (CIA-K) and the flux of magnesium and calcium (CALMAG) as well as mean annual precipitation (MAP) values (Table 1) (Sheldon and Tabor 2009; Nordt and Driese 2010). Molecular weathering ratio values were plotted through each paleosol profile to determine their relative change through the soil profile. Mean values for the molecular weathering ratios and MAP were then calculated for each paleosol profile and plotted from the base to the top of the section at each site.

The relative concentrations of major clay minerals (kaolinite, chlorite, illite, smectite) in 26 paleosol samples were determined by X-ray diffraction (XRD) by K/T Geoservices (Boulder, Colorado). Samples were inserted into a centrifuge and spun separating the clay-sized material. This fraction was then decanted and vacuum filtrated producing oriented mounts which were exposed to ethylene glycol vapor for a 24 h period. A Siemens D500 powder diffractometer with a CuKα radiation source (45 kV, 35 mA) was used to analyze the clay mounts over a range of 2°–36° 2θ at a scan rate of 1°/min to determine the clay mineralogy of the resulting material in weight percent amounts. Clay mineralogy was used to further assess paleoweathering and paleoclimate (Sheldon and Tabor 2009).

Table 1 Molecular weathering ratios and climate proxies, their means of estimation, and significance

Weathering/climate proxy ^a	Equation ^a	Significance ^a
Base loss	$Al_2O_3/(CaO + MgO + Na_2O + K_2O)$	Accumulation of alumina relative to base cations
Hydrolysis (clayeyness)	Al_2O_3/SiO_2	Al accumulates as clay minerals form
Salinization	$Na_2O + K_2O/Al_2O_3$	Accumulation of salts in the subsurface
Calcification	$(CaO + MgO)/Al_2O_3$	Accumulation of Ca, Mg in the subsurface
Leaching (CaO, MgO, Na ₂ O, K ₂ O)	$(CaO, MgO, Na_2O, K_2O)/TiO_2$	Base cations leached during weathering and Ti accumulated in normal conditions
CIA-K	$[(Al_2O_3)/(Al_2O_3 + CaO + Na_2O)] \times 100$	Weathering of feldspars and the formation of clay minerals
MAP (CIA-K)	14.265(CIA-K)-37.632	Estimate of precipitation
CALMAG	$[(Al_2O_3)/(Al_2O_3 + CaO + MgO)] \times 100$	Flux of Ca and Mg from CaCO ₃ , detrital clays, and exchangeable Ca ²⁺ and Mg ²⁺
MAP (CALMAG)	22.69(CALMAG)-435.8	Estimate of precipitation specific to Vertisols

^aModified from Retallack (2001), Sheldon and Tabor (2009) and Nordt and Driese (2010)

3.3 Paleosol analysis and comparisons

Described paleosol sections ($n=21$) were divided into paleosol profiles ($n=40$) based on changes in physical and chemical properties. This included changes in color, rhizohaloes (concentration, color, orientation), mottling (color, concentration), slickenside content, carbonate nodule content, iron concretion content, and microfabric. Paleosol profiles were then grouped into pedotypes based on similar physical and chemical characteristics. Pedotypes are representative of a distinct soil type and soil-forming conditions (Buol et al. 2003). Recognition of pedotypes allows for the analysis of spatial trends in the paleo-landscape resulting from autogenic processes and temporal trends resulting from allogenic processes.

The occurrence of significantly different paleosols in the Monongahela and Dunkard groups was assessed using nonparametric similarity and cluster analysis. This required the quantification of paleosol profile properties (Electronic Supplementary Material Appendix B) including paleosol development (1–5), ichnofabric index (ii) (0–6), carbonate accumulation (0–6), clay accumulation (0–4), slickenside density (0–4), and root density (0–4), as well as molecular weathering ratio values, paleoprecipitation values, and clay mineral concentrations to produce a similarity matrix. The data matrix was imported into PAST 3.16 to run a Bray–Curtis similarity test resulting in a cluster diagram showing which paleosol profiles were most similar and which were most dissimilar.

4 Results

4.1 Sedimentology and stratigraphy

The base of the Monongahela Group consisted of three successions of alternating shale (95–120 cm) and fine- to

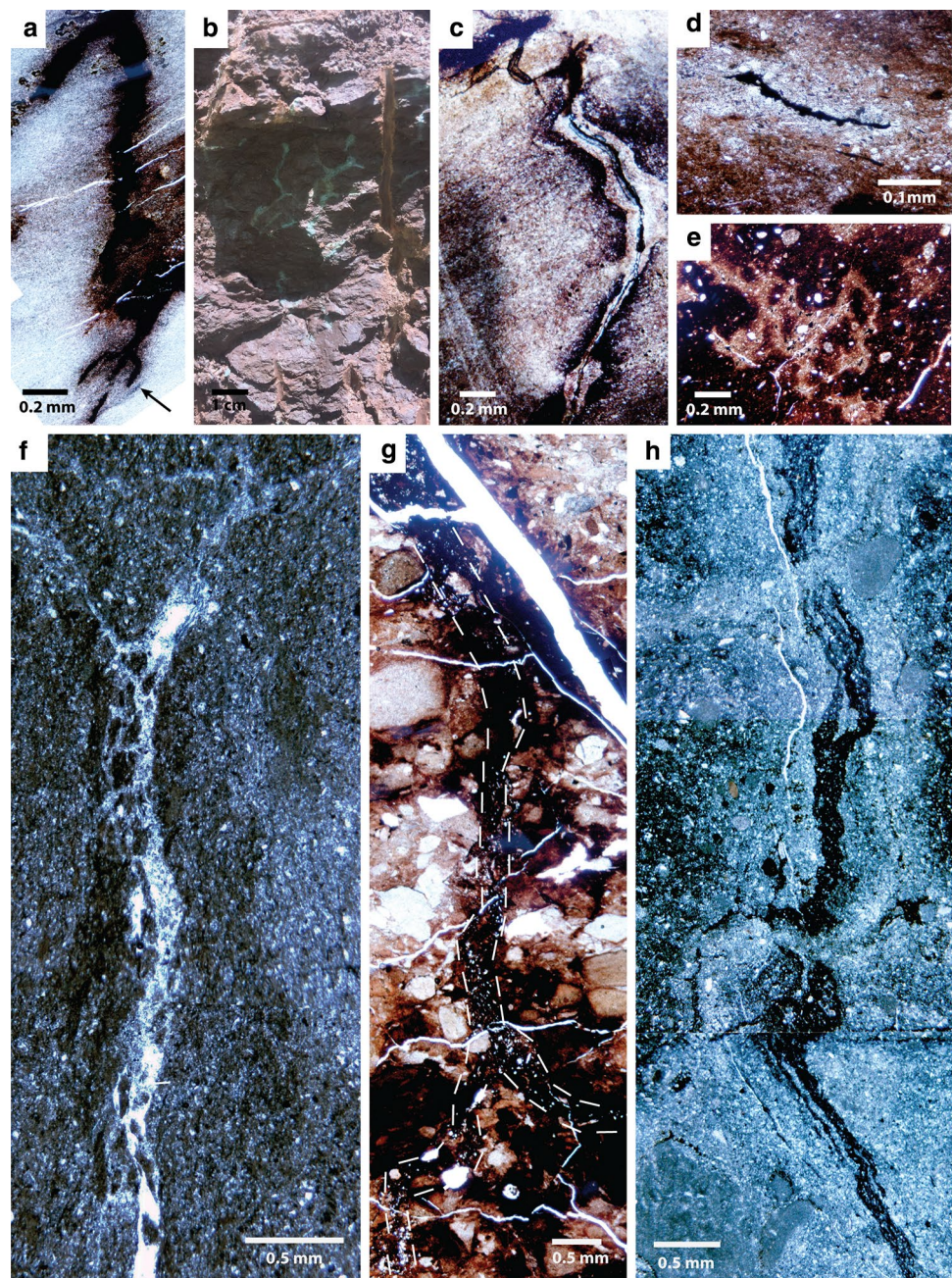
medium-grained, micaceous sandstone (35–130 cm) units (interval A in Fig. 2). These shale-sandstone successions were followed by a mixture of red to grey mudstone (40–86 cm) and micritic limestone (40–185 cm) units for approximately 6 m (interval B in Fig. 2). This interval was followed by five successions of interbedded, fine- to medium-grained, micaceous sandstone and shale (25–170 cm) and grey to red mudstone (30–180 cm) units with one additional limestone bed (70 cm) (interval C in Fig. 2). The upper Monongahela Group consisted of shale (20–190 cm), fine- to medium-grained, thick (210–250 cm) sandstone and thick (160–330 cm) red to purple mudstone units as well as uncommon, conglomerate (43 cm) and limestone (40–70 cm) units (interval D in Fig. 2). The lower Dunkard Group exposed at Sites 1 and 2 began with either a dark grey, fissile shale (Site 1) or a grey, compacted, silty shale (Site 2). After a covered interval was a fine- to coarse-grained sandstone unit (2–5 m thick) (interval E in Fig. 2). The sandstone was followed by six successions of interbedded, grey to red mudstone (35–205 cm) and fine- to coarse-grained, micaceous sandstone (25–170 cm) units and sandy shale (50–270 cm) units (interval F in Fig. 2).

4.2 Continental ichnofossils

4.2.1 Rhizoliths

Rhizoliths observed in outcrop and thin section included abundant rhizohaloes and uncommon root casts (Fig. 3). Rhizohaloes were downward, laterally, or irregularly tapering and branching, commonly grey and rarely yellow or reddish orange, and contained carbonized root cores (Fig. 3a–e). The rhizohaloes had a mean width of 3 mm (0.02–25 mm) and a mean core width of 0.09 mm (0.02–0.28 mm). Thick, cumulative paleosols had the highest abundance of rhizohaloes and simple, underdeveloped paleosols had the lowest.

Fig. 3 Rhizohaloes and root casts. **a** Vertical, grey, branching rhizohaloes from S1P8. **b** Branching, sub-vertical rhizohaloes from S1P7. **c** Vertical, grey rhizohalo from S3P5. **d** Horizontal yellow rhizohalo from S3P6. **e** Complex branching rhizohaloes from S2P3



Gleyed and underdeveloped paleosols more commonly had horizontal rhizohaloes. Rhizohaloes were primarily horizontal from the base to middle of the Monongahela Group, primarily vertical from the top of the Monongahela Group to the beginning of the Dunkard Group, and a mixture of both through the rest of the Dunkard Group. Root casts were present in seven paleosols from Sites 1 and 3 from the middle of the Monongahela Group to the middle of the Dunkard Group. Root casts were widely spaced, vertical to horizontal, branching and non-branching, and passively filled with clay to silt-sized sediment (Fig. 3f–h). Root casts had a mean width of 0.3 mm (0.1–0.8 mm).

4.2.2 Burrows

Common actively filled and rare passively filled fossil burrows were identified within 11 paleosol sections. Passively filled burrows were rare ($n=2$), found in red and reddish purple mudstones, and consisted of vertical, unlined, sharp-walled, branching to non-branching shafts with a mean width of 0.8 mm (0.3–1.3 mm) and a homogeneous, greyish white or brown clay to silt-sized massive fill (Fig. 4a, b). Actively filled burrows ($n=10$) consisted of unlined, sharp-walled, branching to non-branching tunnels and shafts with a mean width of 0.4 mm (0.08–1.2 mm). The active fill consisted of

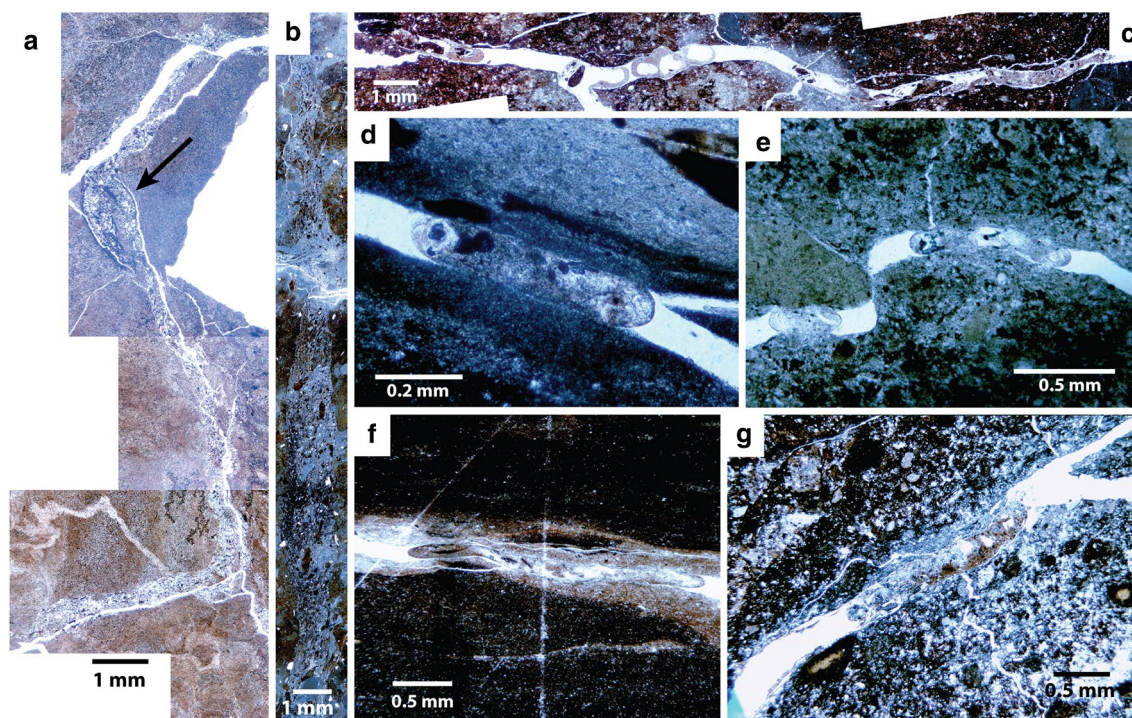


Fig. 4 Burrows. **a** Sub-vertical, branching, passively filled burrow with chamber (at arrow) from S1P6 (cf. *Maconopsis*). **b** Vertical, passively filled burrow from S1P1A (cf. *Planolites*). **c** Horizontal, actively filled burrow from S1P8 (cf. *Taenidium*). **d** Sub-vertical,

actively filled burrow from S3P2B (cf. *Taenidium*). **e** Horizontal, actively filled burrow from S3P2B (cf. *Taenidium*). **f** Horizontal, actively filled burrow from S3P5 (cf. *Taenidium*). **g** Sub-vertical, actively filled burrow from S3P3A (cf. *Taenidium*)

circular to elliptical, light to dark brown, backfills composed of clay to silt-sized sediment (Fig. 4c–g).

4.3 Pedotypes

Forty paleosol profiles were identified and grouped into 11 pedotypes (Figs. 5, 6, 7, Appendices C–E). The Monongahela Group included 26 paleosol profiles divided into nine pedotypes with four unique pedotypes. The Dunkard Group included 14 paleosol profiles divided into seven pedotypes with two unique pedotypes.

4.3.1 Pedotype 1 (PT1) Monongahela and Dunkard groups (Protosols)

PT1 included 37–65 cm thick, complete or incomplete, simple paleosol profiles ($n=5$) classified as Protosols by having weakly developed soil horizons (Mack et al. 1993) (Figs. 5d, h, 7a, h, i, 8a, b). PT1 consisted of dark red, calcareous, blocky to platy mudstone with insepic micro-morphology and porphyroskelic microstructure (Fig. 8c). Ichnofossils included rare to abundant, horizontal to vertical, grey, yellow, and red rhizohaloes, rare horizontal root casts, and rare actively filled burrows ($ii=1$) (Fig. 8d). Slickensides (2–15 cm) were uncommon to common.

Argillans were rare to uncommon. Calcification, salinization, and leaching were low while base loss and hydrolysis were moderate-high (Tables 2, 4). Clay concentrations included low-moderate smectite and moderate-high kaolinite and illite/mica (Table 5).

4.3.2 Pedotype 2 (PT2) Monongahela and Dunkard groups (gleyed Protosols)

PT2 included 20–53 cm thick, incomplete, simple paleosol profiles ($n=3$) classified as gleyed Protosols by having gleyed, weakly developed soil horizons (Mack et al. 1993) (Figs. 5c, 6b, 7b, 8e, f). PT2 was composed of grey blocky to platy mudstone with an insepic to bimasepic microfabric and a porphyroskelic microstructure (Fig. 8g, h). Ichnofossils included rare, small, horizontal, grey and reddish orange rhizohaloes (~ 0.2 cm wide) ($ii=1$). Slickensides (2–10 cm) were uncommon. Argillans, rounded blocky peds, and carbonate nodules were rare (Fig. 8i). Salinization, calcification, Mg- and Ca-leaching were low while hydrolysis and K-leaching were moderate-high (Tables 2, 3, 4). Clay concentrations included low-moderate smectite and moderate-high chlorite and illite/mica (Table 5).

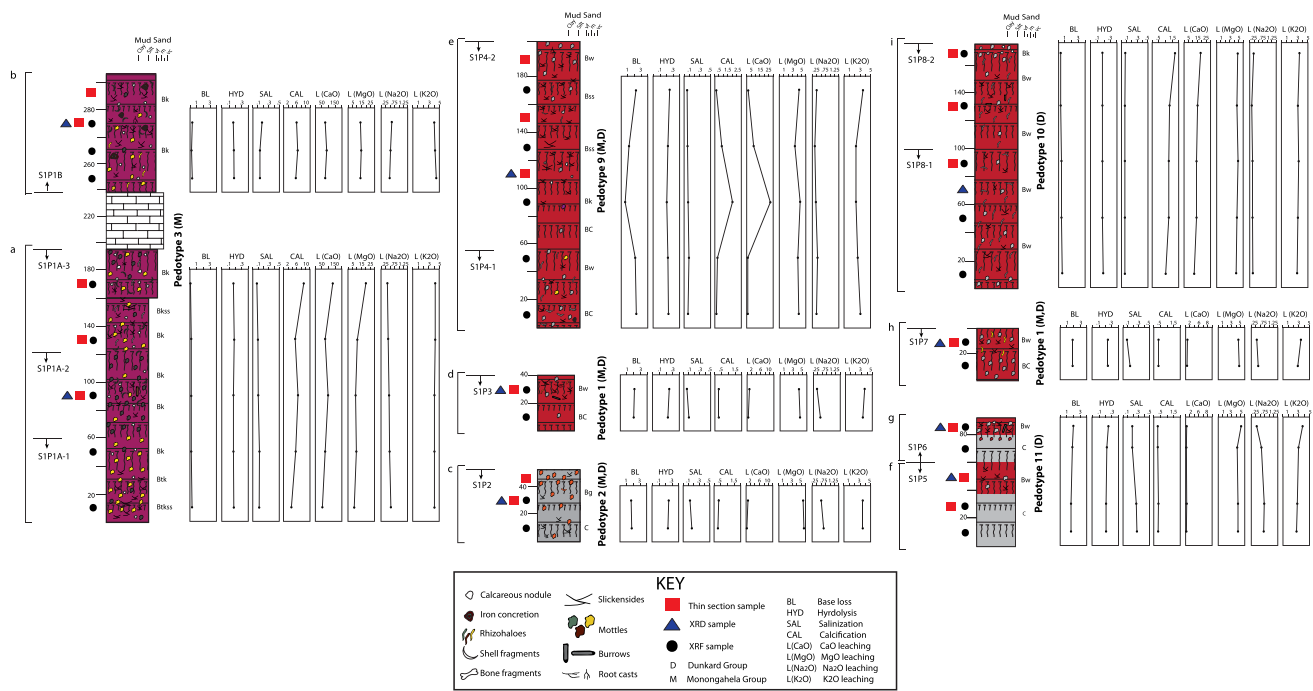


Fig. 5 Detailed paleosol sections from Site 1 (S1P1-S1P8) and plotted molecular weathering ratio values

4.3.3 Pedotype 3 (PT3) Monongahela Group (vertic Calcisols)

PT3 included 40–100 cm thick, incomplete paleosol profiles ($n = 8$) classified as compound to composite, cumulative vertic Calcisols by having over-thickened profiles, prominent calcic soil horizons and slight vertic features with a stacking pattern of profiles separated by layers of minimally weathered sediment (compound) or partially overlapping profiles (composite) (Mack et al. 1993; Kraus 1999) (Figs. 5a, b, 6a, 7c, 8j, k). PT3 consisted of purple to dark red, calcareous, blocky mudstone with a calciasepic microfabric, porphyroskelic to agglomeroplasmic microstructure, angular blocky peds, abundant shell fragments, and rare bone fragments (Fig. 8l–n). Ichnofossils included uncommon, vertical and horizontal, yellow and grey rhizohaloes, rare vertical and horizontal root casts, and rare actively and passively filled burrows ($ii = 2$). Slickensides (0.5–15 cm) were common and argillans were rare to uncommon. Common calcareous nodules (1–2 cm) and rare calcareous concretions (1 cm) occurred in layers. Salinization, base loss and Na-leaching were low-moderate while K-leaching was moderate-high (Tables 2, 3, 4). Clay concentrations included low kaolinite and chlorite and low-moderate smectite and illite/mica (Table 5).

4.3.4 Pedotype 4 (PT4) Monongahela and Dunkard groups (gleyed Calcisols)

PT4 included 50–54 cm thick, incomplete, simple paleosol profiles ($n = 2$) classified as gleyed Calcisols by having prominent calcic soil horizons and gleyed soil profiles (Mack et al. 1993) (Figs. 6d, 7d, 9a–b). PT4 was composed of grey, calcareous, blocky mudstone, a calciasepic to insepic microfabric and a porphyroskelic to agglomeroplasmic microstructure (Fig. 9c). Small (1–4 cm) slickensides were rare to common and argillans rare. Ichnofossils included rare horizontal grey and yellow rhizohaloes (~0.2 cm wide) and actively filled burrows ($ii = 1$). Calcareous nodules (0.5–2 cm) were common. Base loss, salinization, calcification, Mg-, and Na-leaching were low-moderate (Tables 3, 4). Clay concentrations included low-moderate chlorite and moderate-high kaolinite (Table 5).

4.3.5 Pedotype 5 (PT5) Monongahela and Dunkard groups (calcic Vertisols)

PT5 included 40–115 cm thick, incomplete paleosol profiles ($n = 4$) classified as composite to cumulative calcic Vertisols by containing prominent homogenization features from pedoturbation as well as calcic features with a stacking pattern of partially overlapping profiles or over-thickened

Table 2 Site 1 molecular weathering ratios and paleoprecipitation estimates

Pedotype	Sample interval	Horizon	Base loss	Hydrolysis	Salinization	Calcification	Ca leaching	Mg leaching	Na Leaching	K leaching	CIA-K/ CALMAG	MAP
PT10	SIP8 160-175	Bk	0.53	0.18	0.06	1.66	19.79	4.94	0.20	3.29	42.73	572
	SIP8 120-140	Bw	0.60	0.17	0.05	1.44	15.84	4.88	0.16	3.24	47.37	638
	SIP8 80-100	Bw	0.65	0.18	0.05	1.30	14.16	4.94	0.17	3.26	50.59	684
	SIP8 40-60	Bw	0.65	0.18	0.05	1.30	14.47	4.88	0.17	3.25	50.40	681
PT1	SIP8 0-20	Bw	0.81	0.19	0.06	1.02	11.34	4.48	0.18	3.10	57.27	779
	SIP7 20-37	Bw	1.90	0.24	0.08	0.33	0.55	5.49	0.27	3.28	95.70	1328
	SIP7 0-20	BC	1.94	0.24	0.14	0.32	0.43	4.74	0.40	2.86	95.21	1321
PT11	SIP6 20-32	Bw	2.02	0.25	0.07	0.29	0.64	5.36	0.27	3.84	95.73	1328
	SIP6 0-20	C	1.94	0.21	0.18	0.30	0.42	4.23	0.52	2.90	NA	NA
PT11	SIP5 20-40	C	1.80	0.21	0.24	0.33	0.68	4.40	0.67	2.77	NA	NA
	SIP5 0-20	C	1.85	0.21	0.26	0.33	0.45	4.44	0.66	2.55	NA	NA
	SIP4 160-180	Bw	2.18	0.25	0.07	0.27	0.97	4.62	0.23	3.55	78.50	1345
PT9	SIP4 120-140	Bw	1.10	0.21	0.07	0.75	8.27	3.70	0.17	2.40	57.14	861
	SIP4 80-100	Bw	0.45	0.21	0.08	2.06	27.44	4.73	0.19	2.40	32.63	305
	SIP4 40-60	Bw	2.00	0.22	0.10	0.31	0.60	4.43	0.28	2.72	76.18	1293
	SIP4 0-20	BC	2.10	0.24	0.08	0.29	0.67	4.55	0.24	3.10	77.51	1323
PT1	SIP3 20-40	Bw	2.03	0.24	0.07	0.30	1.09	4.34	0.25	3.36	93.21	1292
	SIP3 0-20	BC	1.99	0.23	0.11	0.30	0.64	4.43	0.34	3.18	94.58	1312
PT2	SIP2 20-40	Bg	1.70	0.24	0.15	0.36	1.03	5.61	0.53	3.53	92.10	1276
	SIP2 0-20	C	1.73	0.24	0.18	0.35	0.81	5.73	0.64	3.55	NA	NA
PT3	SIP1B 40-60	Bk	0.16	0.17	0.15	5.96	77.86	14.31	0.63	4.15	16.45	197
	SIP1B 20-40	Bk	0.14	0.17	0.14	6.73	88.84	15.71	0.58	4.20	14.80	174
	SIP1B 0-20	Bk	0.17	0.17	0.13	5.69	74.93	14.82	0.56	4.28	17.28	209
	SIP1A 160-180	Bk	0.11	0.17	0.08	9.17	126.92	20.51	0.34	4.31	11.22	122
SIP1A 120-140	SIP1A 120-140	Bk	0.19	0.18	0.09	5.02	70.02	11.68	0.40	4.29	18.78	230
	SIP1A 80-100	Bk	0.14	0.17	0.10	6.76	95.97	8.96	0.43	4.12	13.87	160
SIP1A 40-60	SIP1A 40-60	Bk	0.18	0.17	0.11	5.17	70.63	9.42	0.47	4.12	17.89	218
	SIP1A 0-20	Btk	0.24	0.18	0.12	3.82	53.60	8.03	0.52	4.16	22.98	290

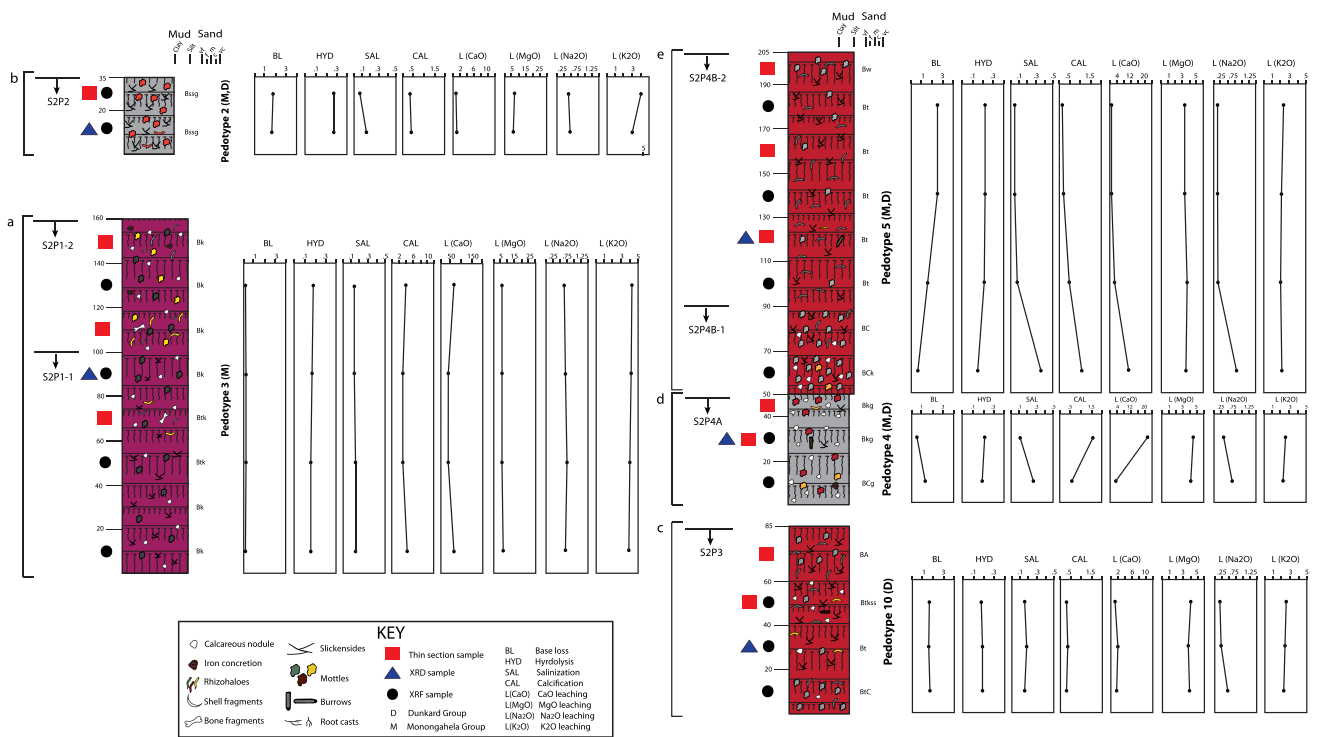


Fig. 6 Detailed paleosol sections from Site 2 (S2P1-S2P4) and plotted molecular weathering ratio values

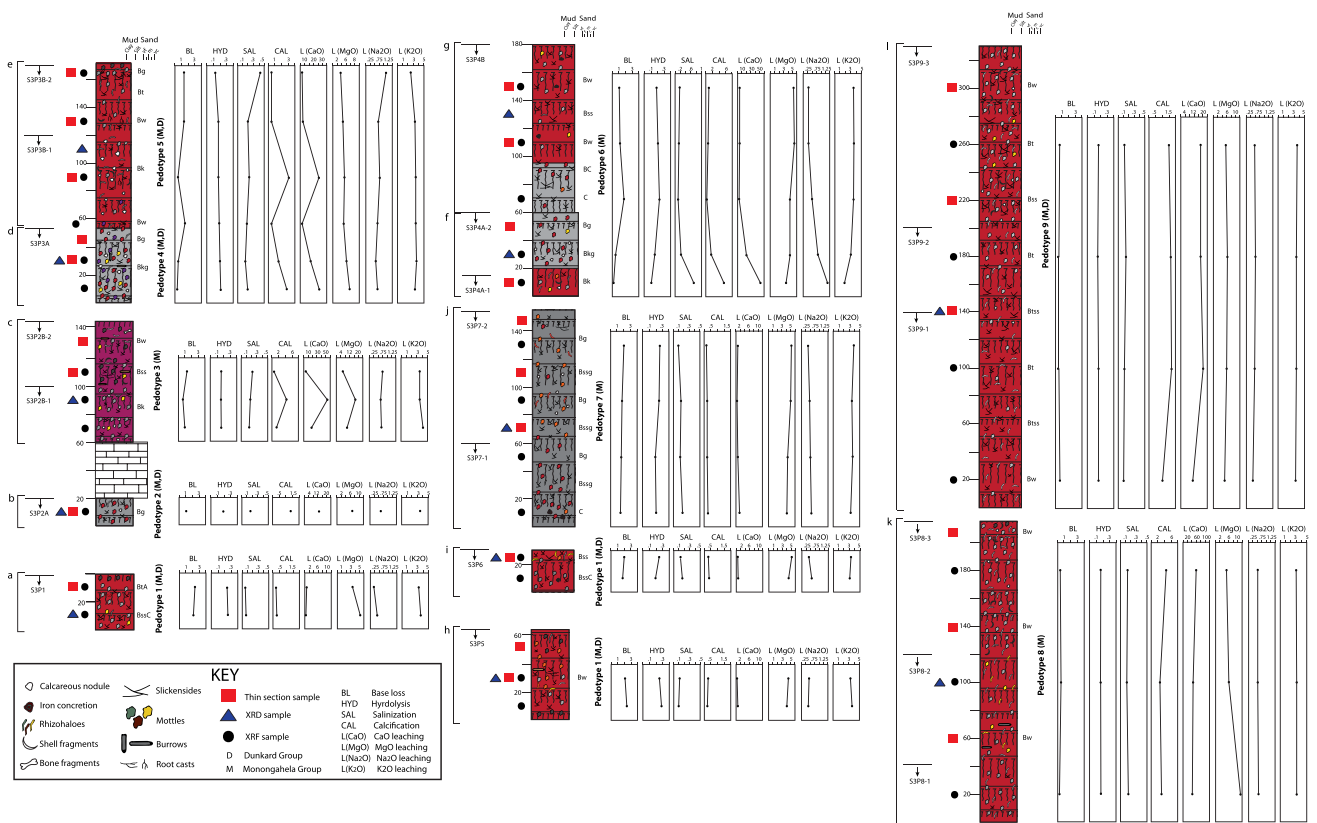


Fig. 7 Detailed paleosol sections from Site 3 (S3P1-S3P9) and plotted molecular weathering ratio values

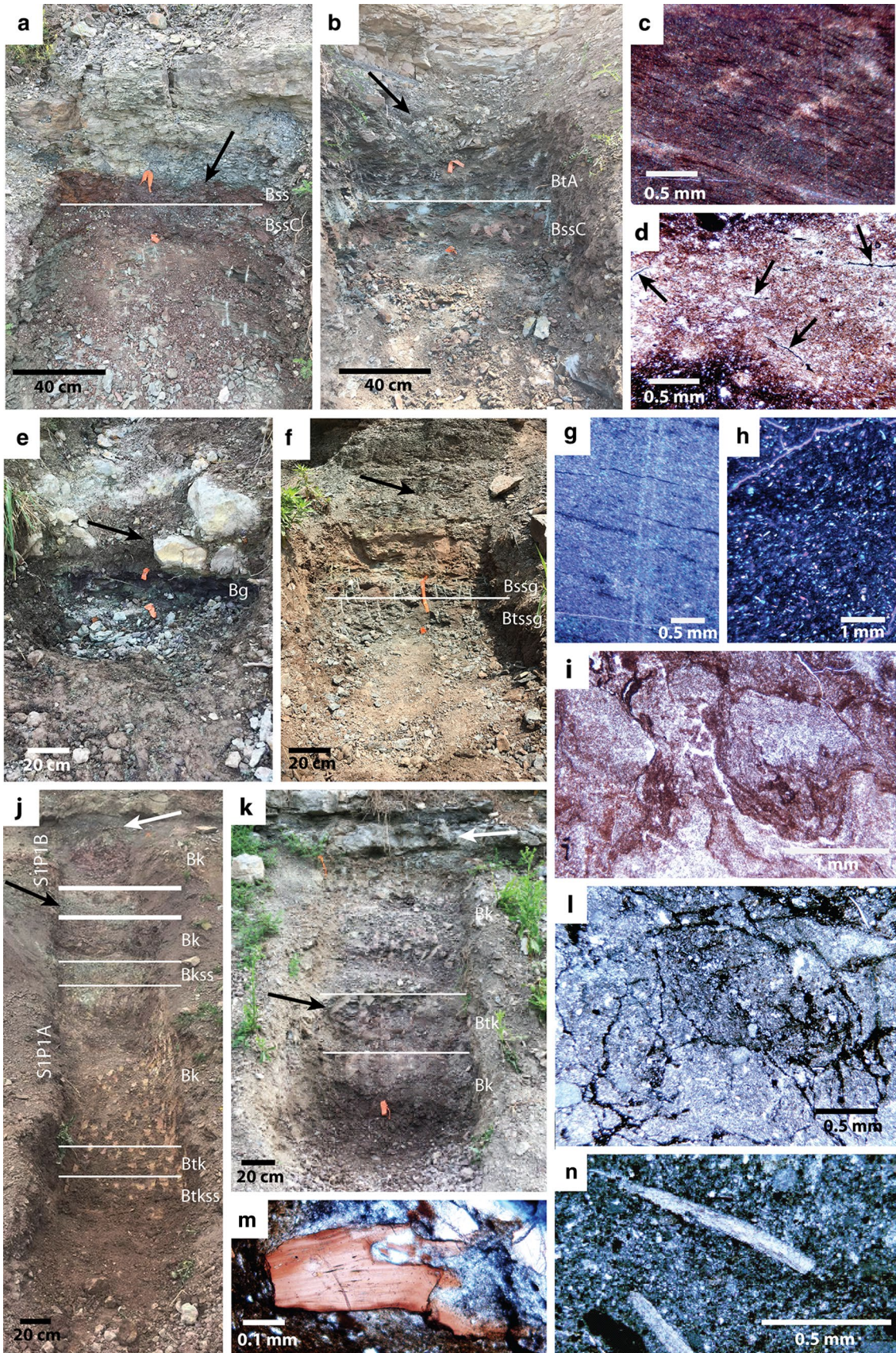


Fig. 8 Pedotype 1. **a** S3P6 paleosol section consisting of platy to blocky, primarily red mudstone with BssC and Bss horizons and overlain by a sharp contact with an interbedded sandstone and shale unit (at arrow). **b** S3P1 paleosol section consisting of red to grey mudstone with BssC and BtA horizons and overlain by a heavily weathered limestone unit (at arrow). **c** Insepic microfabric from S3P6. **d** Cluster of rhizohaloes from S3P6 (at arrows). Pedotype 2. **e** S3P2A paleosol section consisting of blocky, reddish purple to grey mudstone with a Bg horizon and overlain by a limestone unit (at arrow). **f** S2P2 paleosol section consisting of primarily grey, blocky to platy mudstone with Bssg and Btssg horizons overlain by a grey fissile shale unit (at arrow). **g** Bimasepic microfabric from S1P2. **h** Silasepic microfabric from S3P2A. **i** Rounded peds from S2P2. Pedotype 3. **j** S1P1A/B paleosol section consisting of primarily red to purple blocky mudstone with Btk, Bk, and Btkss horizons containing a coarse limestone unit separating two profiles (at black arrow) and overlain by a conglomerate unit (at white arrow). **k** S2P1 paleosol section consisting of red to purple mudstone with Bk and Btk horizons containing large fracture planes in the middle of the profile (at black arrow) and overlain by an interbedded shale and limestone unit (at white arrow). **l** Angular blocky peds from S1P1A. **m** Bone fragment from S3P2B. **n** Shell fragments from S1P1A

profiles (Mack et al. 1993; Kraus 1999) (Figs. 6e, 7e, 9d, e). PT5 was composed of dark red, calcareous, blocky mudstone with an insepic microfabric, porphyroskelic to agglomeroplastic microstructure, rare rounded blocky peds, and shell fragments (Fig. 9f, g). Carbonate cement and nodules (0.9–1.5 cm) were abundant. Slickensides (1–12 cm) and argillans were uncommon to common. Ichnofossils included rare to common, vertical to horizontal, grey and yellow rhizohaloes (~0.3 cm wide), uncommon vertical root casts, and rare actively filled burrows (ii = 5) (Fig. 9f). Hydrolysis, salinization, calcification, and leaching were low-moderate (Tables 3, 4). Clay concentrations included low illite/mica and smectite (Table 5).

4.3.6 Pedotype 6 (PT6) Monongahela Group (vertic Protosols)

PT6 included 20–120 cm thick, incomplete paleosol profiles ($n=3$) classified as compound to composite vertic Protosols by having weakly developed soil horizons with slight vertic features and a stacking pattern of either profiles separated by layers of minimally weathered sediment or partially overlapping profiles (Mack et al. 1993; Kraus 1999) (Figs. 7f–g, 9h–i). PT6 was composed of red to grey, calcareous blocky to platy mudstone with argillasepic to mosepic microfibrils, porphyroskelic microstructure, rare angular blocky peds and shell fragments (Fig. 9j–k). Ichnofossils included rare, vertical and horizontal, grey rhizohaloes (~0.2 cm wide) (ii = 1). Slickensides (1–7 cm) were common. Argillans, calcareous nodules (0.8–3.3 cm), iron concretions (~5 cm), and horizontal fracture planes (~24 cm) were rare. Base loss, hydrolysis, Mg-, and K-leaching were low-moderate (Table 4). Clay concentrations included moderate-high smectite, illite/mica, and chlorite (Table 5).

4.3.7 Pedotype 7 (PT7) Monongahela Group (vertic gleyed Protosols)

PT7 included 60–95 cm thick, incomplete paleosol profiles ($n=2$) classified as composite to cumulative, vertic gleyed Protosols by having weakly developed soil horizons, slight vertic features, gleyed soil profiles, and a stacking pattern containing partially overlapping profiles or over-thickened profiles (Mack et al. 1993; Kraus 1999) (Figs. 7j, 10a). PT7 was composed of a grey, blocky to platy, silty mudstone with a mosepic microfabric, porphyroskelic microstructure, abundant slickensides (1.5–8.5 cm), and rare argillans (Fig. 10b, c). Ichnofossils included rare to uncommon, grey and orange, vertical to subvertical rhizohaloes (~0.2 cm wide), and rare horizontal root casts (ii = 2). Calcareous nodules (~3 cm) were rare to uncommon in the tops of profiles and iron concretions (~4 cm) were rare at the base. Salinization, calcification, Ca-, and Mg-leaching were low (Table 4). Clay concentrations included moderate smectite, kaolinite, and chlorite as well as high illite/mica (Table 5).

4.3.8 Pedotype 8 (PT8) Monongahela Group (Protosols)

PT8 included 40–95 cm thick, incomplete paleosol profiles ($n=3$) classified as composite to cumulative Protosols by having weakly developed soil horizons with a stacking pattern of partially overlapping profiles or over-thickened profiles (Mack et al. 1993; Kraus 1999) (Figs. 7k, 10d). PT8 profiles were composed of a highly calcareous, red, blocky, argillaceous mudstone with a silasepic to insepic microfabric, porphyroskelic microstructure, and common shell fragments. Argillans shifted from rare to common and increased in size (1–30 cm) upward. Ichnofossils included abundant, vertical and horizontal, grey and yellow rhizohaloes (~0.4 cm wide) and rare actively filled burrows (ii = 5) (Fig. 10e–f). Calcareous nodules (~0.6 cm) and slickensides (~4 cm long) were rare. Base loss and salinization were low and K-leaching was high (Table 4). Clay concentrations included low kaolinite, chlorite, and illite/mica and moderate smectite (Table 5).

4.3.9 Pedotype 9 (PT9) Monongahela and Dunkard groups (Vertisols)

PT9 included 60–140 cm thick, incomplete paleosol profiles ($n=4$) classified as compound to composite, cumulative Vertisols by having over-thickened soil horizons with prominent homogenization features from pedoturbation and a stacking pattern consisting of profiles separated by minimally weathered layers (compound) or partially overlapping profiles (composite) (Mack et al. 1993; Kraus 1999) (Figs. 5e, 7l, 10g–h). PT9 profiles were composed of deep red, calcareous, blocky to platy, silty mudstone with

Table 3 Site 2 molecular weathering ratios and paleoprecipitation estimates

Pedotype	Sample interval	Horizon	Base loss	Hydrolysis	Salinization	Calcification	Ca leaching	Mg leaching	Na leaching	K leaching	CIA-K/ CALMAG	MAP
PT5	S2P4B 120-140	Bt	2.59	0.22	0.08	0.25	0.59	3.43	0.17	2.12	80.23	1385
	S2P4B 80-100	Bt	2.50	0.22	0.07	0.26	0.84	3.38	0.15	2.06	79.24	1362
	S2P4B 40-60	Bt	1.62	0.21	0.09	0.47	3.68	3.72	0.18	2.03	67.85	1104
PT4	S2P4B 0-20	Bck	0.77	0.15	0.37	1.09	10.67	3.70	0.77	2.07	47.85	650
	S2P4A 20-40	Bkg	0.55	0.22	0.12	1.64	22.54	4.79	0.33	2.66	42.14	563
	S2P4A 0-20	BCg	1.32	0.19	0.27	0.55	3.93	4.16	0.63	2.35	76.25	1050
PT10	S2P3 40-60	Btkss	1.75	0.18	0.07	0.37	1.35	3.96	0.18	2.78	90.41	1252
	S2P3 20-40	Bt	1.72	0.18	0.08	0.39	1.93	3.68	0.21	2.57	87.08	1205
	S2P3 0-20	BtC	1.78	0.18	0.17	0.38	1.75	3.80	0.39	2.34	87.33	1208
PT2	S2P2 20-35	Bssg	1.87	0.27	0.09	0.34	0.63	6.85	0.34	4.01	95.77	1329
	S2P2 0-20	Bssg	1.75	0.28	0.14	0.38	0.76	6.57	0.45	3.10	94.03	1304
	S2P1 120-140	Bk	0.23	0.17	0.14	4.10	57.51	6.88	0.63	4.37	21.27	266
PT3	S2P1 80-100	Bk	0.28	0.17	0.16	3.29	44.66	6.18	0.66	4.23	25.43	325
	S2P1 40-60	Btk	0.29	0.17	0.17	3.16	42.49	6.75	0.72	4.15	26.48	340
	S2P1 0-20	Bk	0.22	0.16	0.17	4.19	57.24	7.48	0.68	3.98	21.07	263

Table 4 Site 3 molecular weathering ratios and paleoprecipitation estimates

Pedotype	Sample interval	Horizon	Base loss	Hydrolysis	Salinization	Calcification	Ca leaching	Mg leaching	Na leaching	K leaching	CIA-K/ CALMAG	MAP
PT9	S3P9 240-280	Bt	0.56	0.18	0.13	1.51	17.48	5.74	0.49	3.66	39.89	469
	S3P9 160-200	Bt	0.53	0.17	0.15	1.61	17.37	6.26	0.54	3.55	38.38	435
	S3P9 80-120	Bt	0.50	0.17	0.14	1.74	20.02	6.05	0.49	3.53	36.49	392
	S3P9 0-40	Bw	0.76	0.18	0.11	1.07	11.18	5.28	0.37	3.39	48.27	659
PT8	S3P8 160-200	Bw	0.22	0.17	0.14	4.33	60.40	5.50	0.55	3.82	19.98	247
	S3P8 80-120	Bw	0.29	0.17	0.13	3.16	42.49	6.14	0.54	3.99	26.35	338
	S3P8 0-40	Bw	0.26	0.17	0.15	3.48	40.71	11.76	0.60	3.97	26.76	344
	S3P7 120-140	Bg	2.09	0.27	0.11	0.27	0.50	5.27	0.42	3.95	95.82	1329
PT7	S3P7 80-100	Bg	1.89	0.25	0.14	0.31	0.40	4.97	0.48	3.35	95.21	1321
	S3P7 40-60	Bg	1.77	0.20	0.14	0.31	0.66	4.34	0.50	3.68	93.33	1294
	S3P7 0-20	C	1.66	0.20	0.19	0.36	1.90	4.05	0.62	3.28	NA	NA
	S3P6 20-30	Bss	1.93	0.24	0.12	0.31	0.47	5.26	0.42	3.35	95.38	1323
PT1	S3P6 0-20	BssC	1.82	0.19	0.18	0.32	0.58	4.47	0.55	3.05	93.33	1294
	S3P5 20-40	Bw	2.10	0.26	0.13	0.27	0.49	4.61	0.42	3.31	95.30	1322
	S3P5 0-20	Bw	2.45	0.29	0.10	0.22	0.78	4.15	0.39	3.80	95.03	1318
	S3P4B 80-100	Bw	1.06	0.19	0.10	0.69	5.79	5.17	0.36	3.64	71.97	989
PT6	S3P4B 40-60	Bw	1.09	0.21	0.08	0.68	5.89	5.53	0.31	3.71	73.09	1005
	S3P4B 0-20	C	1.84	0.24	0.17	0.33	1.67	4.47	0.59	3.47	NA	NA
	S3P4A 20-40	Bkg	0.53	0.16	0.28	1.63	19.30	4.46	0.83	2.96	41.92	560
	S3P4A 0-20	Bk	0.17	0.10	0.70	5.51	52.72	3.68	1.38	1.98	15.91	189
PT5	S3P3B 106-116	Bg	1.24	0.12	0.43	0.49	2.40	3.72	1.18	2.77	67.03	1085
	S3P3B 66-86	Bw	1.28	0.17	0.21	0.52	3.15	4.71	0.70	3.34	65.93	1060
	S3P3B 26-46	Bk	0.29	0.16	0.22	3.12	41.78	5.48	0.77	3.45	24.30	116
	S3P3B 0-6	Bw	1.47	0.20	0.18	0.43	2.48	4.92	0.67	3.67	70.01	1153
PT4	S3P3A 20-40	Bkg	0.52	0.20	0.15	1.68	23.84	6.00	0.58	3.81	42.16	564
	S3P3A 0-20	Bkg	0.32	0.22	0.20	2.88	42.61	7.99	0.68	3.31	28.87	374
	S3P2B 40-60	Bss	1.01	0.17	0.21	0.72	5.35	5.94	0.75	3.53	72.01	990
	S3P2B 20-40	Bw	0.21	0.17	0.19	4.43	53.41	17.36	0.67	3.58	22.81	288
PT2	S3P2B 0-20	Bk	0.54	0.18	0.16	1.56	17.36	9.64	0.68	4.26	49.02	662
	S3P2A 0-20	Bg	0.66	0.19	0.17	1.27	13.72	7.20	0.61	3.64	53.53	726
PT1	S3P1 20-40	BtA	2.27	0.23	0.07	0.25	0.88	3.44	0.21	3.13	94.08	1304
	S3P1 0-20	BssC	2.02	0.25	0.08	0.30	0.42	5.14	0.27	3.47	96.42	1338

Table 5 Clay mineral concentrations of paleosols from sites 1-3

Sample ID	Pedotype	R0 M-L I/S 90S ^a	R1 M-L I/S 30S ^b	Illite & mica	Kaolinite	Chlorite	Quartz	K-feldspar	Plagioclase	Calcite	Fe dolomite	Goethite	Hematite
Site 1													
S1P8 60-80	PT10	0.0	15.3	13.3	10.9	8.9	9.1	0.8	0.8	18.3	0.0	0.7	21.9
S1P7 30-37	PT1	0.0	10.4	20.7	17.2	19.1	9.2	0.4	2.8	0.2	0.0	2.2	17.8
S1P6 20-32	PT11	0.0	14.3	16.8	17.3	18.4	9.9	0.8	2.5	0.4	0.0	1.1	18.5
S1P5 40-60	PT11	0.0	10.9	19.8	16.0	18.1	9.3	1.0	2.5	0.3	0.0	1.1	21.0
S1P4 100-120	PT9	0.0	5.8	7.2	22.5	8.2	6.5	0.9	1.0	20.2	0.0	2.3	25.4
S1P3 20-40	PT1	0.0	5.7	24.1	20.2	9.9	10.0	1.2	2.9	0.4	0.0	0.0	25.6
S1P2 20-40	PT2	0.0	5.4	36.0	17.4	24.9	11.2	1.1	3.8	0.2	0.0	0.0	0.0
S1P1B 40-60	PT3	0.0	12.8	14.7	1.1	1.9	4.9	2.0	2.5	45.8	3.9	0.0	10.4
S1P1A 80-100	PT3	0.0	7.2	11.6	0.9	1.8	5.1	1.9	1.9	59.4	1.3	2.0	6.9
Site 2													
S2P4B 60-80	PT5	0.0	7.9	12.2	31.5	10.4	10.0	0.5	0.6	0.0	0.0	1.9	25.0
S2P4A 20-40	PT4	0.0	9.1	25.4	30.5	18.5	6.4	0.7	1.3	8.1	0.0	0.0	0.0
S2P3 20-40	PT10	0.0	7.9	16.9	29.6	5.9	11.7	1.3	1.3	0.4	0.0	0.0	25.0
S2P2 0-20	PT2	0.0	8.3	26.8	18.7	29.6	9.9	2.0	4.4	0.3	0.0	0.0	0.0
S2P1 80-100	PT3	0.0	14.3	14.6	1.0	2.9	6.7	0.4	1.0	53.3	0.0	0.0	5.8
Site 3													
S3P9 120-160	PT9	0.0	14.4	13.6	1.9	4.8	15.2	0.5	1.7	35.0	0.0	1.3	11.6
S3P8 80-120	PT8	0.0	15.7	13.5	0.6	1.3	4.9	0.6	1.8	53.8	0.0	0.0	7.8
S3P7 60-80	PT7	0.0	19.2	31.2	15.8	17.2	12.1	1.1	3.1	0.3	0.0	0.0	0.0
S3P6 20-30	PT1	1.5	10.2	28.6	12.2	13.5	9.2	0.9	3.1	0.3	0.0	3.0	17.5
S3P5 20-40	PT1	0.0	8.1	30.1	15.8	18.6	8.7	0.9	3.7	0.3	0.0	2.9	10.9
S3P4B 60-80	PT6	0.0	14.0	32.5	12.7	12.2	7.9	0.5	1.5	4.3	0.0	2.2	12.2
S3P4A 20-40	PT6	13.8	10.2	15.8	16.6	4.7	12.2	1.1	1.6	24.0	0.0	0.0	0.0
S3P3B 46-66	PT5	1.7	4.4	7.3	4.1	1.6	4.0	0.4	0.9	67.7	0.0	0.0	7.9
S3P3A 20-40	PT4	1.3	18.2	22.2	9.7	5.1	9.4	0.5	2.5	15.7	2.7	0.0	12.7
S3P2B 20-40	PT3	1.2	9.1	16.8	5.1	7.7	7.1	0.4	1.6	17.7	23.1	0.6	9.6
S3P2A 0-20	PT2	1.0	13.5	25.2	10.6	9.0	5.1	0.7	2.0	19.2	13.7	0.0	0.0
S3P1 0-20	PT1	0.0	10.2	31.6	28.4	16.9	8.5	0.7	3.2	0.5	0.0	0.0	0.0

^aR0 M-L I/S 90S-R0 Ordered Mixed-Layer Illite/Smectite with 90% Smectite layers^bR1 M-L I/S 30S-R1 Ordered Mixed-Layer Illite/Smectite with 30% Smectite layers

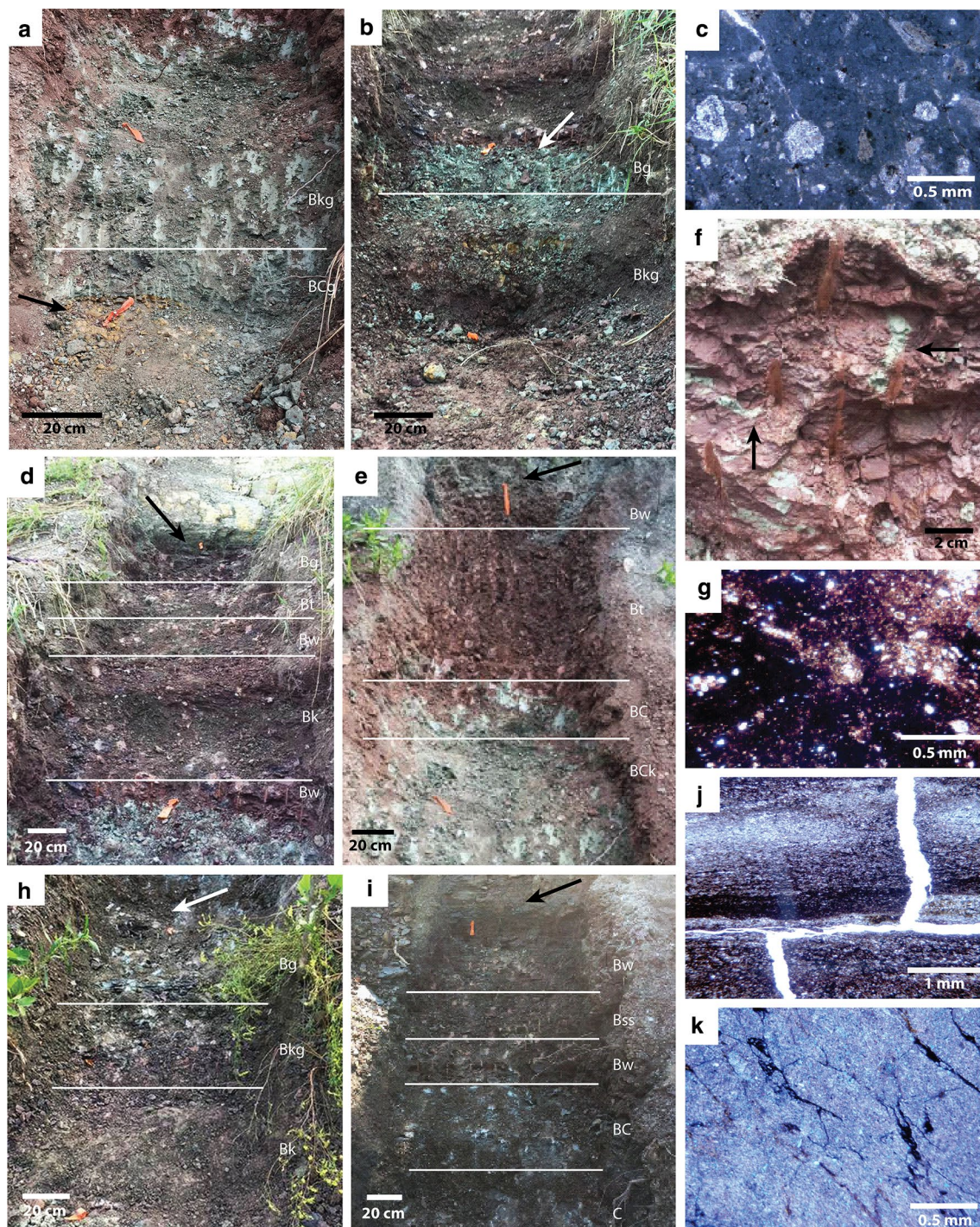
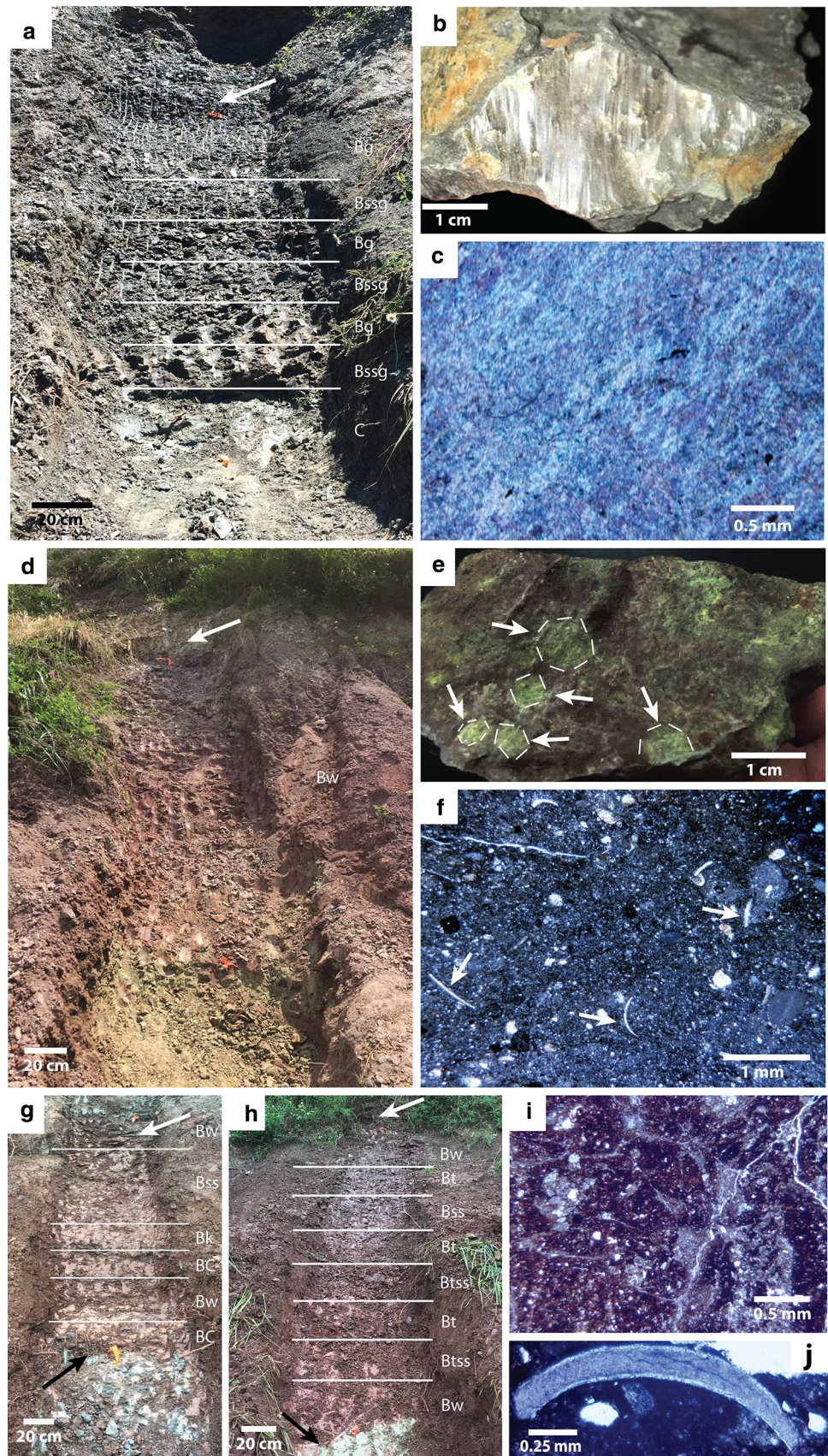


Fig. 9 Pedotype 4. **a** S2P4A paleosol section consisting of primarily grey blocky mudstone including BCg and Bkg horizons with C horizon composed of yellow sandy sediments (at arrow). **b** S3P3A paleosol section consisting of red to grey blocky mudstone with BKg and Bg horizons and a sharp, contact with an overlying paleosol (at arrow). **c** Calciasepic microfabric and agglomeroplasmic microtexture from S3P3A. **d** S3P3B paleosol section consisting of primarily red blocky mudstone with Bw, Bk, Bt, and Bg horizons underlying a gradational contact with a shale unit (at arrow). **e** S2P4B paleosol section consisting of grey to red blocky mudstone with BCK,

BC, Bt, and Bw horizons overlain by a grey fissile shale (at arrow). **f** Vertical and horizontal grey rhizohaloes from S3P3B. **g** Silasepic microfabric from S3P3B. Pedotype 6. **h** S3P4A paleosol section consisting of blocky red to grey mudstone with Bk, Bkg, and Bg horizons overlain by a gradational contact with a C horizon of an overlying paleosol (at arrow). **i** S3P4B paleosol section consisting of grey to red blocky to platy mudstone with C, BC, Bss, and Bw horizons overlain by a ledge-forming, interbedded sandstone and shale unit (at arrow). **j** Argillasepic (laminated) microfabric from S3P4B. **k** Mosepic microfabric from S3P4A

Fig. 10 Pedotype 7. **a** S3P7 paleosol section consisting of grey blocky to play mudstone with Bg, Bssg, and C horizons overlain by a gradational contact with a grey shale unit (at arrow). **b** Slickenside surface from S3P7. **c** Masepic microfabric from S3P7. Pedotype 8. **d** S3P8 paleosol section consisting of a primarily red blocky mudstone with a Bw horizon and an overlying shale unit (at arrow). **e** Cluster of yellow, vertical rhizohaloes in cross section from S3P8. **f** Cluster of shell fragments from S3P8. Pedotype 9. **g** S1P4 paleosol section consisting of primarily red blocky mudstone with Bw, Bss, Bk, and BC horizons, large fracture planes in the upper portion of the section (at white arrow), and underlain by a sharp contact with a grey shale (at black arrow). **h** S3P9 paleosol section consisting of a primarily red blocky mudstone with Bw, Bt, Bss, and Btss horizons underlain by an unconsolidated sandstone unit (at black arrow) and overlain by an argillaceous shale unit (at white arrow). **i** Angular blocky peds from S3P9. **j** Shell fragment from S3P9



insepic microfabrics, a porphyroskelic to granular microstructure, common carbonate nodules, and rare shell fragments (Fig. 10i, j). Slickensides (3–23 cm) were common to abundant, argillans uncommon to abundant, and horizontal breaking planes (30–50 cm) common in the top half of profiles. Ichnofossils included rare to common, vertical and horizontal, grey rhizohaloes (~0.3 cm wide) and rare vertical root casts ($ii = 3$). Salinization, calcification, and leaching were low-moderate while hydrolysis was moderate-high (Tables 2, 4). Clay concentrations included low illite/mica and chlorite and low-moderate smectite (Table 5).

4.3.10 Pedotype 10 (PT10) Dunkard Group (vertic calcic Protosols)

PT10 included 75–100 cm thick, complete to incomplete paleosol profiles ($n = 3$) classified as simple or cumulative-composite, vertic calcic Protosols by having weakly developed soil horizons with slight vertic and calcic features composed of either a simple, single profile or partially overlapping, over-thickened profiles (Mack et al. 1993; Kraus 1999) (Figs. 5i, 6c, 11a–c). PT10 was composed of dark red, blocky to platy, calcareous mudstone with an insepic to mosepic microfabric, porphyroskelic microstructure, rare angular blocky peds, and rare iron concretions (Fig. 11d, e). Slickensides (1–8.5 cm) and argillans were uncommon to common (Fig. 11f). Ichnofossils included abundant, vertical to horizontal, grey and yellow rhizohaloes (~0.4 cm wide) and rare actively filled burrows ($ii = 4$). Calcareous nodules (0.3–2.3 cm) were rare to common. Salinization, base loss, calcification, and leaching were low-moderate while hydrolysis was moderate (Tables 2–3). Clay concentrations included low-moderate smectite, illite/mica, and chlorite and moderate-high kaolinite (Table 5).

4.3.11 Pedotype 11 (PT11) Dunkard Group (Protosols)

PT11 included 32–60 cm thick, incomplete, simple paleosol profiles ($n = 2$) classified as compound Protosols by having weakly developed soil horizons and a stacking pattern of profiles separated by minimally weathered layers (Mack et al. 1993; Kraus 1999) (Figs. 5f–g, 11g–h). PT11 was composed of light grey to red, blocky to platy mudstone with a mosepic microfabric, porphyroskelic microstructure, and rare iron nodules (~0.3 cm) (Fig. 11i). Slickensides (1.5–7 cm) were common and argillans rare (Fig. 11j). Ichnofossils included rare passively filled burrows ($ii = 1$). Calcification, salinization and leaching were low-moderate while base loss and hydrolysis were moderate-high (Table 2). Clay minerals concentrations included moderate smectite, chlorite, kaolinite, and illite/mica (Table 5).

4.4 Trends in molecular weathering ratios

Molecular weathering ratios of the paleosols displayed different degrees of variation through the Monongahela to Lower Dunkard section (Fig. 12, Tables 6, 7). Base loss varied throughout the section (0.11–2.60), starting high at the base and ending with more uniform, low to moderate values at the top. Hydrolysis was generally uniform through the section (0.10–0.29), starting moderate at the base and ending with moderate to high values. Salinization varied throughout the section (0.05–0.70), but started and ended with uniform and low values. Calcification values varied greatly (0.22–9.10), starting low and ending with non-uniform, low to moderate values. Ca-leaching (0.40–127), Mg-leaching (0.15–20.50), Na-leaching (0.15–1.38), and K-leaching (2.0–4.40) all varied through the section. Paleosols at the base of the section had low to moderate Ca-leaching values and low to high values for Mg-leaching, Na-leaching, and K-leaching. At the top of the section Ca-leaching and Na-leaching were low to moderate, Mg-leaching was low, and K-leaching was moderate.

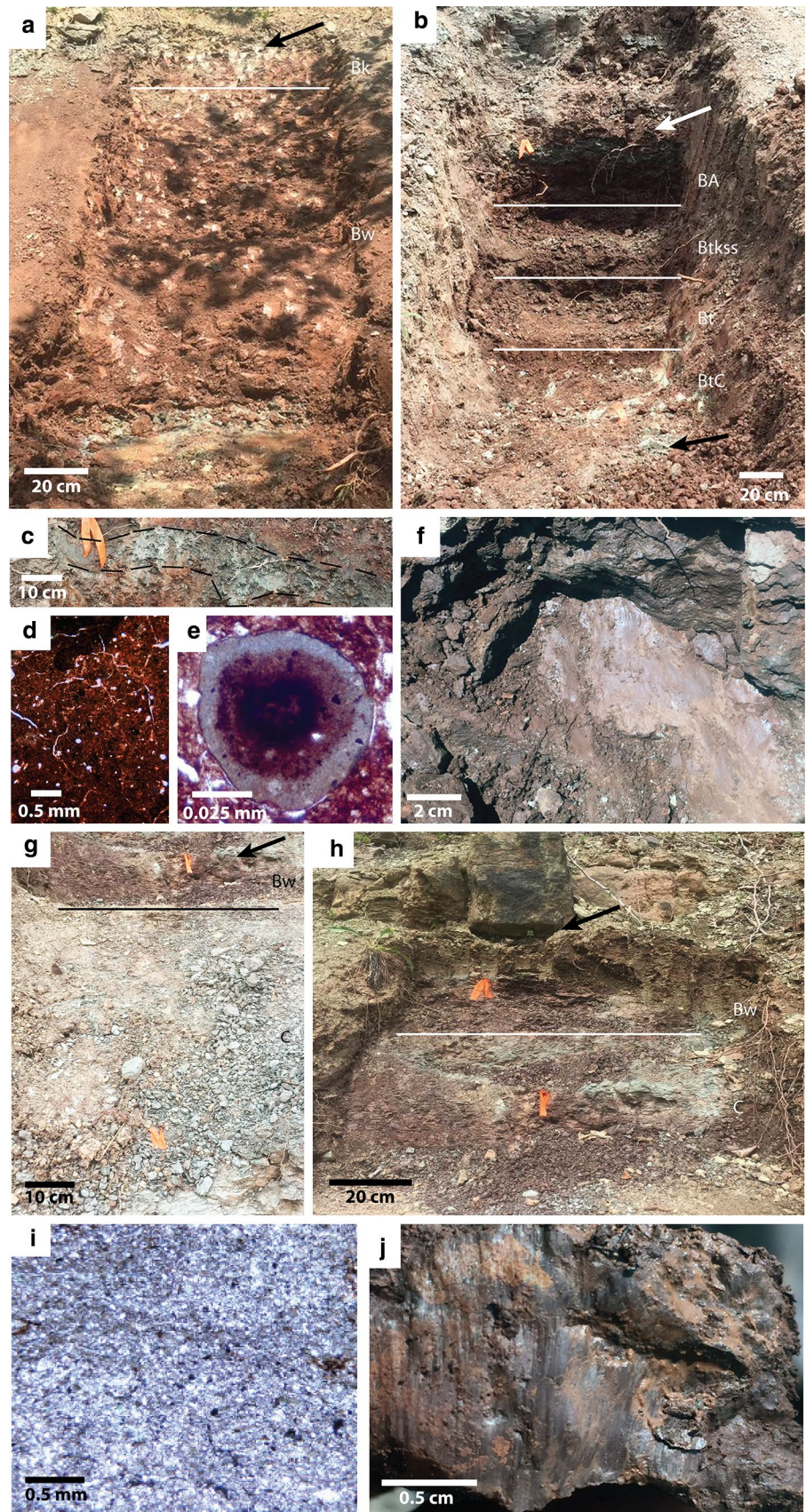
4.5 Trends in clay mineralogy

Clay mineral concentrations in paleosols varied through the Monongahela to Lower Dunkard section (Fig. 13, Tables 5, 6). Smectite ranged from 4.0 to 24.0%, starting and ending with moderate concentrations. Illite/mica ranged from 7.2 to 36.0%, starting high at the base of the section and ending with low to moderate concentrations. Kaolinite ranged from 0.6 to 32%, starting high and ending with moderate concentrations. Chlorite varied from 1.3 to 30.0%, starting moderate and ending with moderate to low concentrations.

4.6 Paleosol comparison and analyses

The data matrix of paleosol properties was used to compare all of the paleosol sections using the Bray–Curtis similarity test (Table 8, Electronic Supplementary Material Appendix F). The resulting cluster diagram produced three major groups of paleosol sections with a similarity > 0.72 (Fig. 14). Group 1 was composed of four paleosol sections from the Monongahela Group representing two pedotypes with a relative similarity of 0.79. PT8 was unique to group 1. Group 2 included six paleosol sections from the Monongahela Group and one from the Dunkard Group representing six pedotypes with a similarity > 0.73. PT3 and PT4 were unique to group 2. Group 3 included six paleosol sections from the Monongahela Group and nine from the Dunkard Group representing nine pedotypes with a similarity of > 0.73. PT1, PT5, PT7, and PT11 were unique to group 3.

Fig. 11 Pedotype 10. **a** S1P8 paleosol section consisting of blocky to platy, primarily red mudstone with Bk and Bw horizons and overlain by a sharp contact with a sandy shale (at arrow). **b** S2P3 paleosol section consisting of a blocky, primarily red mudstone with BA, Btkss, Bt, and BtC horizons overlain by a sharp contact with a red to grey shale (at white arrow) and underlain by a sandstone unit (at black arrow). **c** Outlined view of A horizon preserved in S2P3. **d** Angular blocky pedis from S2P3. **e** Cross section view of iron concretions from S1P8. Pedotype 11. **f** Large slickenside surface from S1P8. **g** S1P5 paleosol section consisting of grey to red, blocky to platy mudstone with Bw and C horizons sharply contacted by the C horizon of the overlying paleosol (at arrow). **h** S1P6 paleosol section consisting of grey to red blocky to platy mudstone with Bw and C horizons overlain by ledge-forming sandstone unit (at arrow). **i** Thin section image of C horizon from S1P5. **j** Slickenside surface from S1P6



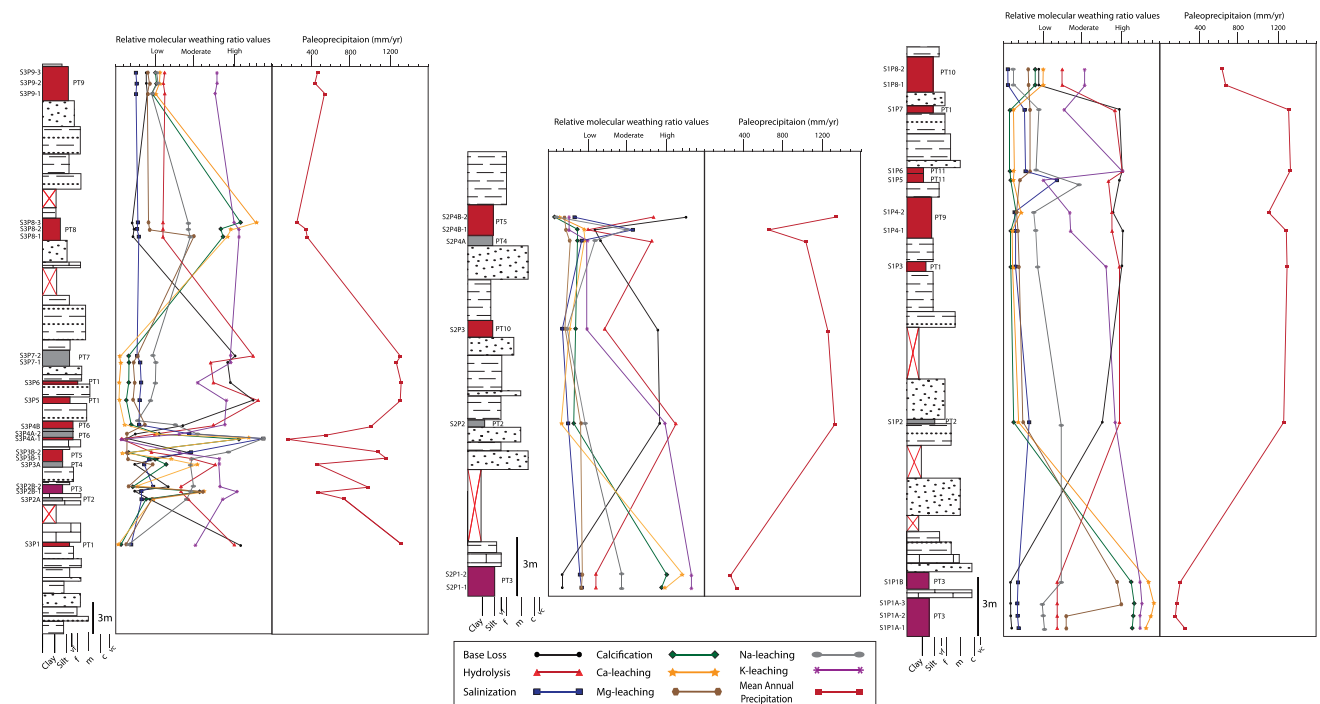


Fig. 12 Relative changes in median molecular weathering ratio values and MAP for each paleosol from the Monongahela to Lower Dunkard groups

Table 6 High to low ranges for molecular weathering ratio values calculated in study

	Low	Moderate	High
Base loss	0.1–0.7	0.8–2.0	2.1–2.6
Hydrolysis	0.1–0.2	0.2–0.24	0.25–0.29
Salinization	0.1–0.2	0.2–0.5	0.5–0.7
Calcification	0.2–1.5	1.6–3.9	4.0–9.2
Ca-leaching	0.4–15.9	16.0–45.0	45.1–60.0
Mg-leaching	3.4–7.5	7.6–16.0	16.1–20.5
Na-leaching	0.2–0.5	0.6–1.0	1.1–1.4
K-leaching	2.0–2.6	2.7–3.8	3.9–4.4
Smectite	5–10	11–20	21+
Illite/Mica	7–14	15–29	30+
Kaolinite	1–9	10–24	25+
Chlorite	1–9	10–24	25+

5 Discussion

5.1 Paleoenvironmental interpretations of pedotypes

Analysis of the properties of the 11 established pedotypes allowed for the interpretation of different aspects of the paleolandscape such as local paleotopography, local

paleohydrology, sedimentation rates, landscape stability, and duration of exposure (Kraus 1999; Birkeland 1999; Retallack 2001; Kraus and Hasiotis 2006; Sheldon and Tabor 2009; Trendall et al. 2013).

5.1.1 Pedotype 1 (PT1) landscapes

PT1 profiles represent Lithic Dystrudepts (Inceptisols) which form under an udic soil moisture regime and have a lithic contact within 50 cm of the soil surface (Soil Survey Staff 2014). PT1 profiles included BA, BtA, Bw, Bss, BC, and BssC horizons whose microfabric, color, mottling, slickensides, and rare rhizoliths indicated immature soils formed under alternating wetting and drying cycles (Schaetzl and Anderson 2005; Tabor and Poulsen 2008). Estimated MAP (~ 1300 mm/yr) suggested wet conditions. Elevated base loss, hydrolysis, and kaolinite indicated a hot and humid climate and generally high soil moisture (Schaetzl and Anderson 2005; Sheldon and Tabor 2009). Truncation of A horizons by sandstone or shale and the immaturity of the paleosols indicated PT1 profiles formed with exposure times of ~ 10¹–10² years on relatively unstable and mildly seasonal proximal floodplains prone to either channel switching or water ponding (Fig. 15) (Birkeland 1999; Kraus 1999; Sheldon and Tabor 2009).

Table 7 Median molecular weathering ratio values and MAP values for each paleosol

Paleosol	Base loss	Hydrolysis	Salinization	Calcification	Ca leaching	Mg leaching	Na leaching	K leaching	CIA-K/ CAL- MAG	MAP
Site 3										
S3P9-3	0.56	0.18	0.13	1.51	17.48	5.74	0.49	3.66	39.89	469
S3P9-2	0.55	0.17	0.14	1.56	17.43	6.00	0.52	3.60	39.14	452
S3P9-1	0.63	0.18	0.12	1.41	15.60	5.66	0.43	3.46	42.38	526
S3P8-3	0.22	0.17	0.14	4.33	60.40	5.50	0.55	3.82	19.98	247
S3P8-2	0.29	0.17	0.13	3.16	42.49	6.14	0.54	3.99	26.35	338
S3P8-1	0.26	0.17	0.15	3.48	40.71	11.76	0.60	3.97	26.76	344
S3P7-2	1.99	0.26	0.12	0.29	0.45	5.12	0.45	3.65	95.51	1325
S3P7-1	1.77	0.20	0.14	0.31	0.66	4.34	0.50	3.68	93.33	1294
S3P6	1.88	0.22	0.15	0.32	0.53	4.87	0.48	3.20	94.36	1308
S3P5	2.28	0.28	0.11	0.25	0.64	4.38	0.41	3.55	95.17	1320
S3P4B	1.07	0.20	0.09	0.69	5.84	5.35	0.33	3.67	72.53	997
S3P4A-2	0.53	0.16	0.28	1.63	19.30	4.46	0.83	2.96	41.92	560
S3P4A-1	0.17	0.10	0.70	5.51	52.72	3.68	1.38	1.98	15.91	189
S3P3B-2	1.26	0.14	0.32	0.50	2.78	4.22	0.94	3.05	66.48	1073
S3P3B-1	0.88	0.18	0.20	1.77	22.13	5.20	0.72	3.56	47.16	1153
S3P3A	0.42	0.21	0.18	2.28	33.22	7.00	0.63	3.56	35.52	469
S3P2B-2	1.01	0.17	0.21	0.72	5.35	5.94	0.75	3.53	72.01	990
S3P2B-1	0.38	0.17	0.17	2.99	35.39	13.50	0.68	3.92	35.91	475
S3P2A	0.66	0.19	0.17	1.27	13.72	7.20	0.61	3.64	53.53	726
S3P1	2.14	0.24	0.07	0.27	0.65	4.29	0.24	3.30	95.25	1321
Site 2										
S2P4B-2	2.50	0.22	0.08	0.26	0.84	3.43	0.17	2.06	79.24	1362
S2P4B-1	0.77	0.15	0.37	1.09	10.67	3.70	0.77	2.07	47.85	650
S2P4A	0.94	0.21	0.20	1.10	13.23	4.48	0.48	2.51	59.19	1050
S2P3	1.75	0.18	0.08	0.38	1.75	3.80	0.21	2.57	87.33	1206
S2P2	1.81	0.28	0.11	0.36	0.70	6.71	0.39	3.56	94.90	1316
S2P1-2	0.23	0.17	0.14	4.10	57.51	6.88	0.63	4.37	21.27	266
S2P1-1	0.28	0.17	0.17	3.29	44.66	6.75	0.68	4.15	25.43	325
Site 1										
S1P8-2	0.60	0.17	0.05	1.44	15.84	4.88	0.16	3.24	47.37	638
S1P8-1	0.65	0.18	0.05	1.30	14.16	4.88	0.17	3.25	50.59	684
S1P7	1.92	0.24	0.11	0.32	0.49	5.11	0.33	3.07	95.46	1324
S1P6	2.02	0.25	0.07	0.29	0.64	5.36	0.27	3.84	95.73	1328
S1P5	1.83	0.21	0.25	0.33	0.57	4.42	0.67	2.66	NA	NA
S1P4-2	1.64	0.23	0.07	0.51	4.62	4.16	0.20	2.97	67.82	1103
S1P4-1	2.05	0.23	0.09	0.30	0.64	4.49	0.26	2.91	76.84	1308
S1P3	2.01	0.24	0.09	0.30	0.87	4.39	0.29	3.27	93.90	1302
S1P2	1.70	0.24	0.15	0.36	1.03	5.61	0.53	3.53	92.10	1276
S1P1B	0.16	0.17	0.14	5.96	77.86	14.82	0.58	4.20	16.45	197
S1P1A-3	0.15	0.18	0.09	7.09	98.47	16.10	0.37	4.30	15.00	176
S1P1A-2	0.14	0.17	0.10	6.76	95.97	8.96	0.43	4.12	13.87	160
S1P1A-1	0.21	0.18	0.12	4.49	62.12	8.73	0.49	4.14	20.44	254

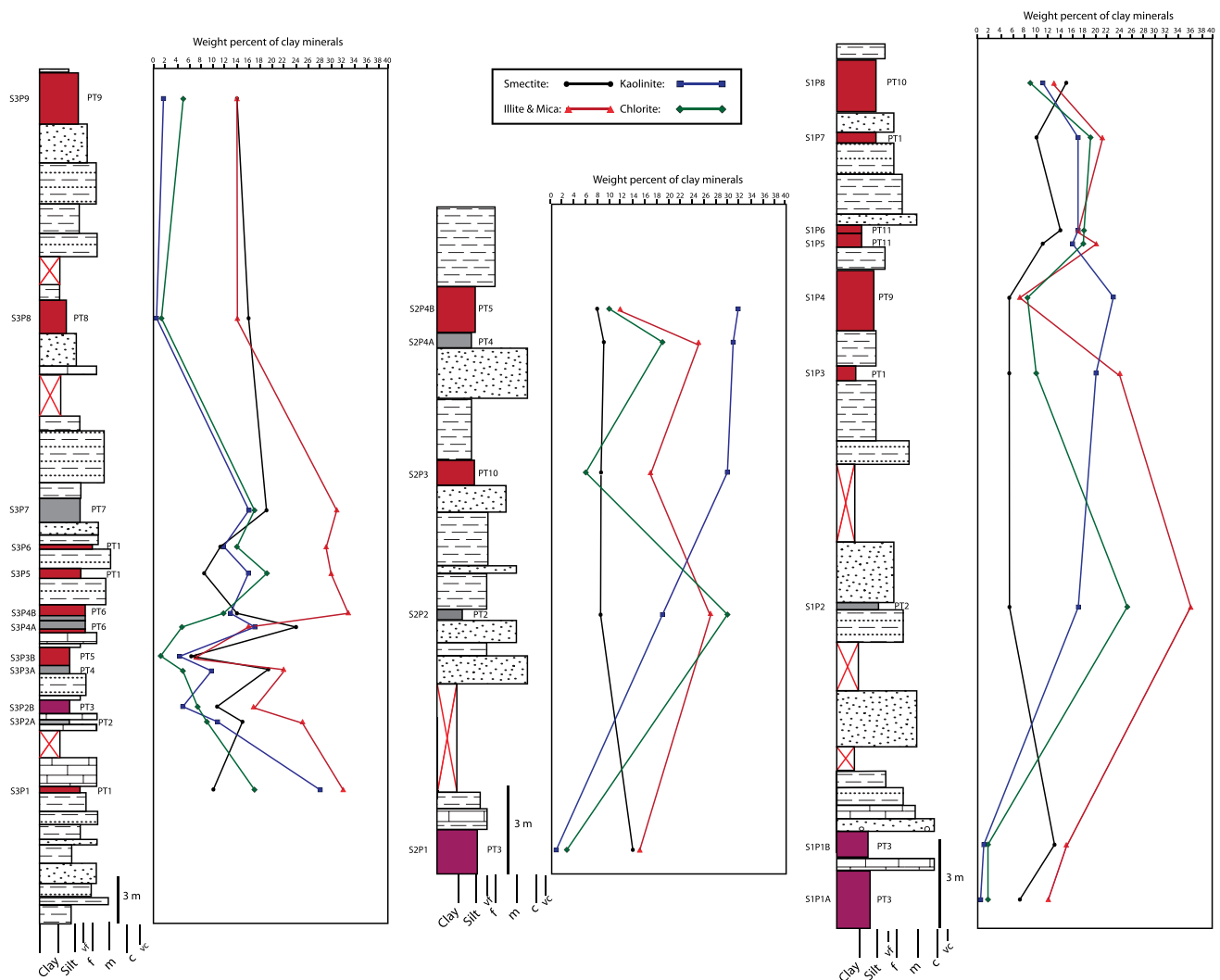


Fig. 13 Relative changes in clay mineral concentrations for each paleosol from the Monongahela to Lower Dunkard groups

5.1.2 Pedotype 2 (PT2) landscapes

PT2 profiles represent Endoaquepts (Inceptisols) which possess redoximorphic features and are fully saturated at some time during the year (Soil Survey Staff 2014). PT2 profiles included Bg, Btg, Bssg, and C horizons whose color, mottling, common slickensides, and rare carbonate nodules suggested some wet and dry seasonality (Buol et al. 2003; Schaetzl and Anderson 2005). Primarily horizontal rhizohaloes and insepic to silasepic microfibrils indicated prolonged waterlogged conditions and poor soil development (Retallack 2001; Kraus and Hasiotis 2006). Estimated MAP yielded high values (~ 1200 mm/year) and low levels of leaching and high levels of hydrolysis indicated poorly-drained conditions (Schaetzl and Anderson 2005). PT2 profiles likely formed on seasonally dry waterlogged proximal floodplains with exposure times of ~ 10¹–10³ years (Fig. 15) (Kraus 1999; Retallack 2001; Hasiotis 2002).

5.1.3 Pedotype 3 (PT3) landscapes

PT3 profiles represent Calcustepts (Inceptisols) which form under an rustic soil moisture regime and have a calcic horizon within 100 cm of the soil surface (Soil Survey Staff 2014). PT3 profiles included Bk, Bkss, Btk, Btkss, and Bw horizons whose color reflected the presence of organics, manganese oxides, and hematite (PiPujol and Buurman 1994; Wright et al. 2000). Seasonal conditions with prolonged dry seasons and variable soil moisture regimes were indicated by gley mottling, horizontal to vertical rhizohaloes, common slickensides, carbonate nodules, and iron concretions (Marriott and Wright 1993; Schaetzl and Anderson 2005; Kraus and Hasiotis 2006; Tabor and Poulsen 2008). Estimated MAP (~ 300 mm/year) was the second lowest of all pedotypes. Profile stacking patterns indicated that sedimentation shifted from being rapid and unsteady to slow and steady over

Table 8 Paleosol property values used in Bray Curtis similarity test

Paleosol	Development (1-5)	Ichnofabric index (0-6)	Carbonate accumulation (0-6)	Clay accumulation (0-4)	Slickenside density (0-4)	Root density (0-4)	ClA-K	Base loss	Salinization	Calcification	Ca leaching	Mg leaching	Na leaching	K leaching	Hydrolysis	Kaolinite	Smectite	Chlorite	K-Feld/Plag-Feld	Illite/Mica
SIPIA	3	2	2	1	2	2	16.9	0.2	0.1	6.0	83.4	11.7	0.4	4.2	0.2	0.9	7.2	1.8	1.0	11.6
SIPIB	3	1	2	2	3	2	16.2	0.2	0.1	6.1	80.5	14.9	0.6	4.2	0.2	1.1	12.8	1.9	0.8	14.7
SIP2	2	1	0	1	1	1	92.1	1.7	0.2	0.4	1.0	5.6	0.5	3.5	0.2	17.4	5.4	24.9	0.3	36.0
SIP3	1	1	0	1	3	2	93.2	2.0	0.1	0.3	1.1	4.3	0.2	3.4	0.2	20.2	5.7	9.9	0.4	24.1
SIP4	2	3	1	2	3	3	72.7	1.4	0.1	0.9	9.3	4.4	0.2	2.8	0.2	22.5	5.8	8.2	0.9	7.2
SIP5	1	1	0	1	3	2	75.3	1.8	0.3	0.3	0.6	4.4	0.7	2.7	0.2	16.0	10.9	18.1	0.4	19.8
SIP6	3	1	1	1	3	0	95.7	2.0	0.1	0.3	0.6	5.4	0.3	3.8	0.3	17.3	14.3	18.4	0.3	16.8
SIP7	2	3	0	1	3	3	95.7	1.9	0.1	0.3	0.5	5.5	0.3	3.3	0.2	17.2	10.4	19.1	0.1	20.7
SIP8	3	4	3	2	1	4	49.7	0.7	0.1	1.3	15.1	4.8	0.2	3.2	0.2	10.9	15.3	8.9	1.0	13.3
S2P1	3	2	2	3	1	2	23.6	0.3	0.2	3.7	50.5	6.8	0.7	4.2	0.2	1.0	14.3	2.9	0.4	14.6
S2P2	1	1	1	2	4	1	94.9	1.8	0.1	0.4	0.7	6.7	0.4	3.6	0.3	18.7	8.3	29.6	0.5	26.8
S2P3	3	5	3	4	3	4	88.7	1.7	0.1	0.4	1.6	3.8	0.2	2.7	0.2	29.6	7.9	5.9	1.0	16.9
S2P4A	3	1	3	2	1	1	42.1	0.6	0.1	1.6	22.5	4.8	0.3	2.7	0.2	30.5	9.1	18.5	0.5	25.4
S2P4B	3	4	2	4	2	3	90.0	2.2	0.1	0.3	1.7	3.5	0.3	2.1	0.2	31.5	7.9	10.4	0.8	12.2
S3P1	2	1	0	4	2	1	94.1	2.3	0.1	0.2	0.9	3.4	0.2	3.1	0.2	28.4	10.2	16.9	0.2	31.6
S3P2A	2	1	1	3	3	1	53.5	0.7	0.2	1.3	13.7	7.2	0.6	3.6	0.2	10.6	14.5	9.0	0.4	25.2
S3P2B	3	5	1	1	4	3	47.9	0.6	0.2	2.2	25.4	11.0	0.7	3.8	0.2	5.1	10.3	7.7	0.3	16.8
S3P3A	3	2	3	1	2	1	42.2	0.3	0.2	1.7	23.8	6.0	0.6	3.8	0.2	9.7	19.5	5.1	0.2	22.2
S3P3B	3	4	2	3	2	4	67.1	1.1	0.3	1.1	12.5	4.7	0.8	3.3	0.2	4.1	6.1	1.6	0.4	7.3
S3P4A	3	1	2	1	3	1	28.9	0.4	0.5	3.6	36.0	4.1	1.1	2.5	0.1	16.6	24.0	4.7	0.7	15.8
S3P4B	3	1	0	1	3	1	72.5	1.1	0.1	0.7	5.8	5.4	0.3	3.7	0.2	12.7	14.0	12.2	0.3	32.5
S3P5	2	2	0	3	3	2	95.2	2.3	0.1	0.2	0.6	4.4	0.4	3.6	0.3	15.8	8.1	18.6	0.2	30.1
S3P6	2	2	0	1	4	3	95.4	1.9	0.1	0.3	0.5	5.3	0.4	3.4	0.2	12.2	11.7	13.5	0.3	28.6
S3P7	4	2	1	1	3	2	94.8	1.9	0.1	0.3	0.5	4.9	0.5	3.7	0.2	15.8	19.2	17.2	0.4	31.2
S3P8	4	5	1	1	1	4	24.4	0.3	0.1	3.7	47.9	7.8	0.6	3.9	0.2	0.6	15.7	1.3	0.3	13.5
S3P9	4	4	1	4	3	4	47.6	0.6	0.1	1.5	16.5	5.8	0.5	3.5	0.2	1.9	14.4	4.8	0.3	13.6

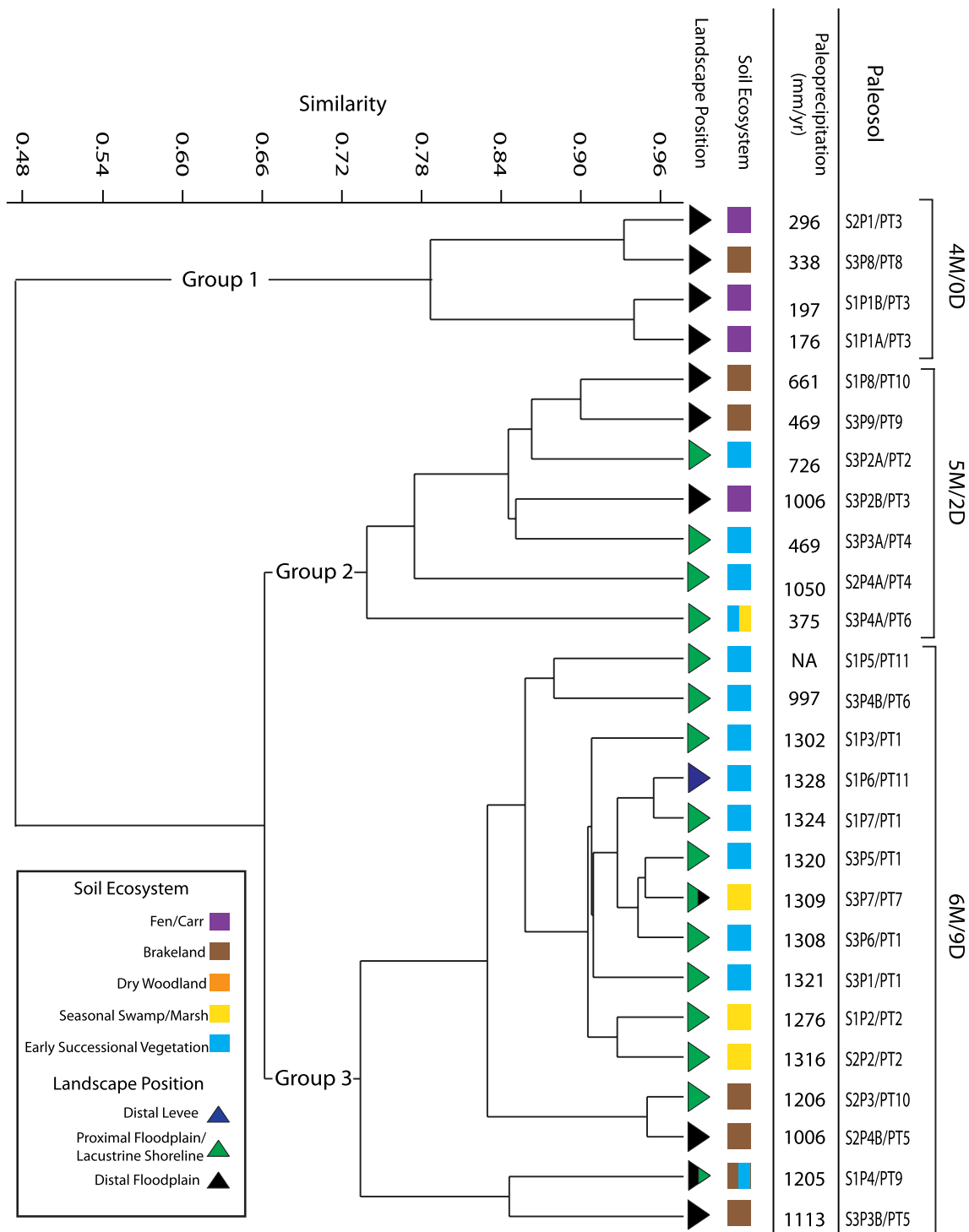


Fig. 14 Bray Curtis similarity test cluster diagram with plotted landscape position, soil ecosystem, and paleoprecipitation values. Each node is labeled with the paleosol (e.g., S2P1) and its pedotype (e.g., PT3). *M* Monongahela Group, *D* Dunkard Group

time (Kraus 1999). PT3 properties indicated high levels of soil development with exposure times of $\sim 10^4$ – 10^5 years (Marriott and Wright 1993; Birkeland 1999). Abundant calcareous nodules and a calciasepic microfabric in

combination high organic content suggested that PT3 profiles likely formed on a low-lying distal floodplain with standing alkaline water similar to a fen (Fig. 15) (Motzkin 1994; Retallack 2001).

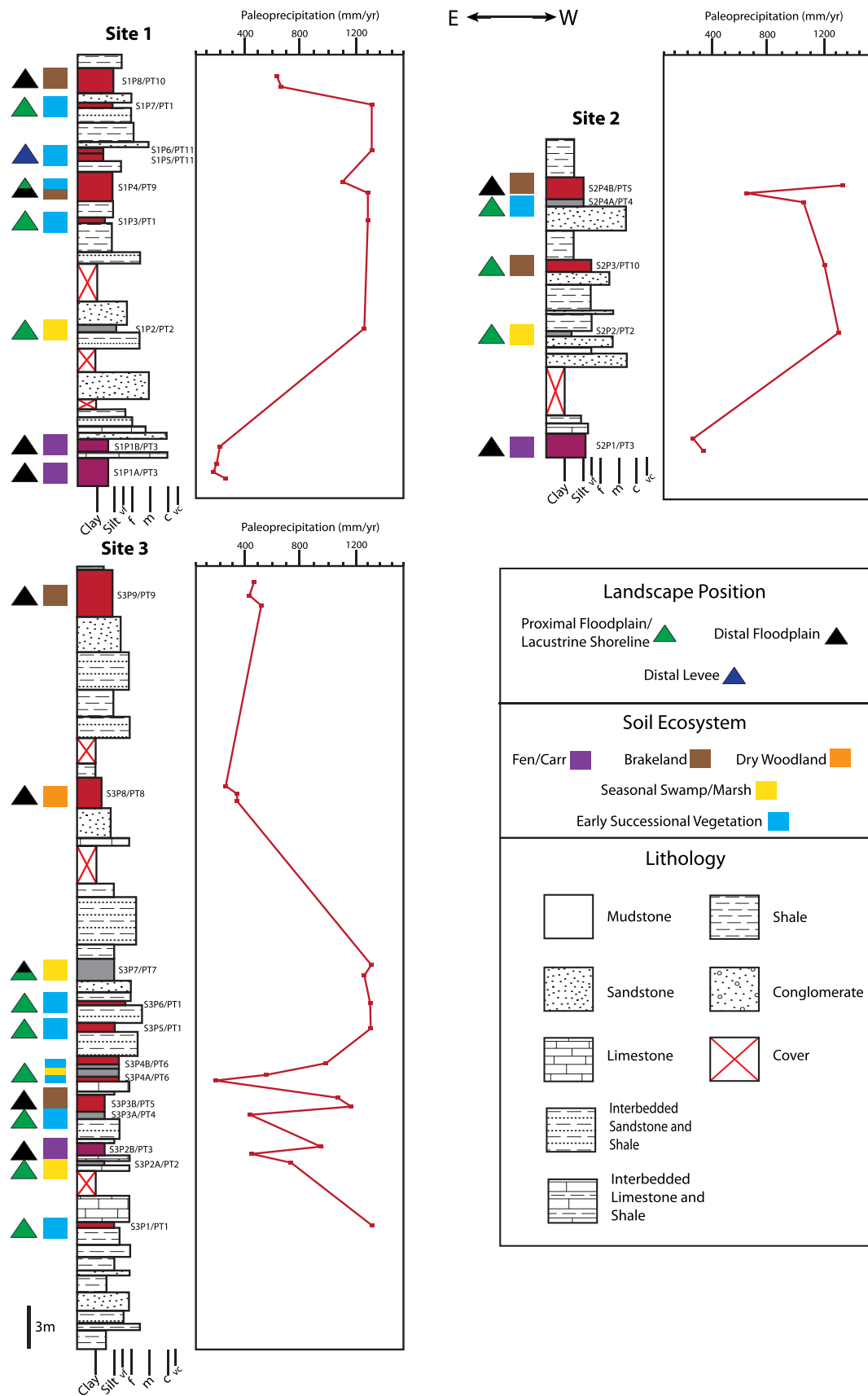


Fig. 15 Interpreted changes in landscape position, soil ecosystems, and paleoprecipitation values for each paleosol throughout the complete section

5.1.4 Pedotype 4 (PT4) landscapes

PT4 profiles represent Eutrudepts (Inceptisols) which form in an udic soil moisture regime and have free carbonates throughout (Soil Survey Staff 2014). PT3 profiles included all gleyed horizons (Bg, Bkg, BCg) suggesting waterlogged conditions, while red mottles, common slickensides, and calcareous nodules indicated the profiles were seasonally dry (Kraus 1999; Schaetzl and Anderson 2005). The occurrence of rhizohaloes and burrows only near the top of profiles suggested a generally high water table (Retallack 2001). Estimated MAP (~640 mm/year) was moderate to low relative to other pedotypes. Low base loss values combined with high kaolinite concentrations indicated a hot and humid landscape (Retallack 2001; Sheldon and Tabor 2009). Limited ichnofossils, high carbonate concentration, and indications of poor soil development from an exposure time of 10^1 – 10^2 years suggested that PT4 profiles formed on unstable, relatively dry proximal floodplains with gleization attributed to flooding causing temporary poorly-drained conditions (Birkeland 1999; Kraus 1999; Retallack 2001) (Fig. 15).

5.1.5 Pedotype 5 (PT5) landscapes

PT5 profiles represent Calcicusterts (Vertisols) which have cracks open for at least 90 days per year and a calcic horizon within 100 cm of the surface (Soil Survey Staff 2014). PT5 profiles included Bw, Bt, Bk, Bg, BC, and BCk horizons whose red matrix, grey mottles, shallow-to-deep root casts, large slickensides, and calcareous nodules indicated strongly seasonal conditions with a fluctuating water table (Marriott and Wright 1993; Buol et al. 2003; Tabor and Poulsen 2008; Sheldon and Tabor 2009). Profile stacking patterns indicated formation where either sedimentation was steady to unsteady, but exceeded by pedogenesis (Kraus 1999). Estimated MAP (~1200 mm/year) was high. Rounded blocky peds, slickensides, carbonate nodules, and vertical rhizohaloes indicate high soil development and a relatively stable landscape (Birkeland 1999; Retallack 2001; Hasiotis 2002). PT5 profiles were estimated to have an exposure time of 10^3 – 10^4 years and developed on a distal floodplain under temporally varying moisture regimes (Fig. 15) (Birkeland 1999; Kraus 1999; Hasiotis 2002).

5.1.6 Pedotype 6 (PT6) landscapes

PT6 profiles represented Eutrudepts (Soil Survey Staff 2014) composed of Bw, Bk, Bkg, Bss, Bg, BC, and C horizons whose color, slickensides, calcareous nodules, and iron concretions indicated fluctuating soil moisture (Marriott and Wright 1993; Kraus 1999; Schaetzl and Anderson 2005; Tabor and Poulsen 2008). Clay concentrations suggested a cool and dry seasonal climate (Sheldon and Tabor

2009). Estimated MAP (~1000 mm/year) was moderate. PT6 development was interpreted to be poor with exposure times of $\sim 10^1$ – 10^2 years based on the rare rhizohaloes, variable microfabric, thick C to BC horizons, relict bedding, and dispersed slickensides (Birkeland 1999; Retallack 2001). Profile stacking patterns indicated they formed where sedimentation was unsteady and rapid to moderate (Kraus 1999). Based on poor soil development, profile thickness, and fluctuating moisture, PT6 profiles were interpreted as forming on unstable proximal floodplains with temporary transitions to a seasonal swamp (Fig. 15) (Kraus 1999; Retallack 2001; Hasiotis 2002).

5.1.7 Pedotype 7 (PT7) landscapes

PT7 profiles represented Endoaquepts (Inceptisols) (Soil Survey Staff 2014) containing Bg, Bssg, and C horizons indicating mostly reducing processes (Kraus 1999; Schaetzl and Anderson 2005). Extensive gleization, red rhizohaloes, iron concretions, calcareous nodules, and slickensides suggested alternation of anoxic surface water ponding causing reducing soil conditions and surface drying resulting in well-drained, oxidizing soil conditions (PiPujol and Buurman 1994; Buol et al. 2003; Kraus and Hasiotis 2006). Estimated MAP (~1300 mm/year) was high. Profile stacking patterns indicated sedimentation was moderate and unsteady, but exceeded by pedogenesis (Kraus 1999). Mosaic microfabrics, uniform molecular weathering ratios, and slickensides throughout suggested moderate development in a marsh environment situated in a transitional zone between the proximal and distal floodplain with exposure times of $\sim 10^2$ – 10^3 years (Fig. 15) (Birkeland 1999; Kraus 1999; Retallack 2001).

5.1.8 Pedotype 8 (PT8) landscapes

PT8 profiles represented Haplustepts (Inceptisols) forming in a rustic soil moisture regime (Soil Survey Staff 2014). PT8 included red Bw horizons, calcareous nodules, slickensides, deep vertical rhizohaloes and backfilled burrows indicating a well-drained soil with a seasonal distribution of moisture and a stable, low water table (Marriott and Wright 1993; Buol et al. 2003; Kraus and Hasiotis 2006). Estimated MAP (~300 mm/year) was the low. Profile stacking patterns indicated formation where sedimentation was slow and steady to moderate and unsteady (Kraus 1999). Calcification, leaching, and base loss values as well as kaolinite concentration were consistent with a dry climate (Retallack 2001). Microfabric, deep rhizohaloes, carbonate nodules, and cumulative profiles suggested moderate soil development on a stable distal floodplain with exposure times of 10^2 – 10^3 years (Fig. 15) (Kraus 1999; Retallack 2001).

5.1.9 Pedotype 9 (PT9) landscapes

PT9 profiles represented Haplusterts (Vertisols) which have cracks open for at least 90 days per year (Soil Survey Staff 2014). PT9 profiles included mostly red Bw, Bss, Bt, Btss, Bk and BC horizons with slickensides, carbonate nodules, and vertical to horizontal rhizohaloes indicating seasonal conditions resulting in alternating well- and poorly-drained soil conditions (Kraus 1999; Schaetzl and Anderson 2005; Kraus and Hasiotis 2006). Molecular weathering ratios suggested a seasonally wet environment (Sheldon and Tabor 2009). Estimated MAP (~700 mm/year) was moderate, but varied among profiles (~300–1300 mm/yr). Profile stacking patterns indicated sedimentation shifted from rapid to slow (Kraus 1999). Microfabrics and pedogenic properties suggested poor to moderate development with exposure times of ~ 10^2 – 10^4 years on distal floodplains that experienced seasonally wet conditions with rare, dry periods (Fig. 15) (Kraus 1999; Retallack 2001; Hasiotis 2002).

5.1.10 Pedotype 10 (PT10) landscapes

PT10 profiles represented Eutrudepts (Inceptisols) (Soil Survey Staff 2014) with mostly red BA, Bw, Bt, Bk, Btkss BC, and, BtC horizons containing slickensides, calcareous nodules, iron concretions, and deep rhizohaloes suggesting a seasonal climate with a distinct dry season resulting in well-drained soil conditions and a low water table (Kraus 1999; Schaetzl and Anderson 2005; Kraus and Hasiotis 2006). Estimated MAP (~850 mm/year) was moderate. Kaolinite concentration indicated high soil moisture and a hot and humid environment (Sheldon and Tabor 2009). Profile stacking patterns indicated moderate to slow sedimentation (Kraus 1999). Cumulative profiles and their properties indicated moderately-developed soils forming on distal floodplains with exposure times of 10^3 – 10^4 years (Fig. 15) (Kraus 1999; Retallack 2001).

5.1.11 Pedotype 11 (PT11) landscapes

PT11 profiles represented Dystrudepts (Inceptisols) (Soil Survey Staff 2014) containing red Bw horizons with slickensides and carbonate nodules indicated seasonally dry conditions and a well-drained soil (Kraus 1999; Schaetzl and Anderson 2005). The thin profiles and absence of ichnofossils suggested little time for plants and animals to colonize due to frequent burial by flooding events (Kraus 1999; Hasiotis 2002). High base loss and hydrolysis indicated a saturated, but well-drained soil (Retallack 2001, Schaetzl and Anderson 2005). Estimated MAP (~1300 mm/yr) was high. Profile stacking patterns indicated rapid and unsteady sedimentation (Kraus 1999). Thin soil profiles with thick C horizons and an absence of ichnofossils indicated

poor development with an estimated exposure time of 10^1 – 10^2 years on distal levees (Fig. 15) (Kraus 1999; Retallack 2001; Hasiotis 2002).

5.2 Soil ecosystems

Pedogenic properties, body fossils, and trace fossils allowed for the interpretation of five different ecosystems represented by the paleosols of the Monongahela and Dunkard groups. The observed ichnofossil assemblages are interpreted as representing the *Scoyenia* (wet/dry) and *Coprinisphaera* (dry) ichnofacies (Genise et al. 2000; Buatois and Mángano 2011).

5.2.1 Ecosystem 1 (Early successional vegetation)

Ecosystem 1 included PT1, PT4, PT6 (S3P4A-1, S3P4B), PT9 (S1P4-2), and PT11 whose rhizoliths reflected patchy vegetation resulting from fluctuations in water table depths as well as mostly poorly-drained conditions (Retallack 2001; Kraus and Hasiotis 2006). Rarity of rhizoliths was attributed to either too little time for plant development (~10 years) or the occurrence of frequent disturbance events such as floods (Kimmins 1997; Retallack 2001). Actively filled burrows were similar to *Taenidium* and interpreted as deposit feeding burrows of soil arthropods suggesting a moderately to well-drained soil (moisture content of 5–45%) (D'Alessandro and Bromley 1987; Smith and Hasiotis 2008; Smith et al. 2008). Passively filled burrows with chambers were similar to *Macanopsis* and interpreted as dwelling or reproduction burrows of soil arthropods based on their size (Buatois and Mángano 2011; Hembree and Nadon 2011; Mikas and Uchman 2013; Hembree and Bowen 2017). Ecosystem 1 included early successional vegetation consisting of herbaceous plants that colonized bare ground situated on distal levee to proximal floodplain environments (Fig. 15) (Retallack 2001; Buol et al. 2003).

5.2.2 Ecosystem 2 (Clastic swamp/marsh)

Ecosystem 2 included PT2, PT6 (S3P4A-2), and PT7 whose rhizoliths indicated a patchier distribution of vegetation than ecosystem 1 and mostly poorly-drained conditions (Retallack 2001; Kraus and Hasiotis 2006). Vegetation likely consisted of low diversity assemblages of lycopsids, pteridophytes and small ferns tolerant of standing water with a seasonal component excluding peat formation (DiMichele et al. 2001; Retallack 2001). Absence of burrows is a result of the waterlogged soils (Buatois and Mángano 2011). Ecosystem 2 likely consisted of either a clastic swamp such as a seasonally waterlogged forest or a clastic marsh consisting of herbaceous plants in acidic freshwater (Fig. 15) (Retallack 2001; Buol et al. 2003).

5.2.3 Ecosystem 3 (Fen)

Ecosystem 3 included PT3 profiles with abundant rhizoliths. Vegetation was likely adapted to wet and wet/dry environments and included shallow to moderately rooted herbaceous plants in addition to lycopsids, pteridosperms, and tree ferns (Motzkin 1994; Pfefferkorn and Wang 2009; DiMichele et al. 2001; Kiviat 2010). Actively filled burrows (*Taenidium*) were attributed to locomotion and feeding by soil arthropods. Passively filled vertical burrows were similar to *Planolites* and interpreted as the product of detritus or deposit feeding of larval or adult arthropods (Buatois and Mángano 2011; Hembree and Nadon 2011). The presence of both passive and actively filled burrows indicated at least intermittently moderate soil moisture conditions favorable for soil animals (Retallack 2001). Abundant ostracode valves and rare bone fragments of amphibians or fish suggested some standing water at the surface. These paleosols likely formed on a strongly seasonal, saturated distal floodplain similar to a fen consisting of herbaceous or woody wetland vegetation rooted in pooled alkaline water (Fig. 15) (Retallack 2001; Buol et al. 2003; Hembree and Bowen 2017).

5.2.4 Ecosystem 4 (Brakeland)

Ecosystem 4 included PT5, PT9 (S1P4-1, S3P8-1-S3P8-3) and PT10 profiles whose rhizoliths suggested cycles of oxidizing and reducing conditions (Retallack 2001; Kraus and Hasiotis 2006). Vegetation, including pteridosperms, would have been tolerant of seasonal conditions including enhanced dry seasons, yet grew on a stable landscape with ample time to develop (DiMichele et al. 2001; Eble et al. 2001; Retallack 2001). *Taenidium* were interpreted as locomotion and feeding burrows of soil arthropods. Ecosystem 4 consisted of brakelands containing extensive herbaceous vegetation such as ferns growing in a well-drained soil situated on a distal floodplain (Fig. 15) (Retallack 2001; Buol et al. 2003).

5.2.5 Ecosystem 5 (Dry woodland)

Ecosystem 5 included PT8 whose rhizoliths suggested a shift from well-drained to moderately drained conditions over time (Retallack 2001). Vegetation likely consisted of conifers, callipterids, and other plants adapted to seasonally dry conditions (DiMichele et al. 2001). The occurrence of *Taenidium* along with abundant root traces suggested the use of roots as a food source similar to the larva of many types of extant insects (Smith and Hasiotis 2008). PT8 profiles most likely developed in a dry woodland situated on a distal floodplain (Fig. 15) (Retallack 2001; Buol et al. 2003).

5.3 Landscape evolution and climate change from Late Pennsylvanian to Early Permian

Throughout the studied section autogenic processes, generally related to changing sedimentation rates and hydrology associated with channel proximity, had an influence on soil development. However, these local-scale controls were overprinted by significant allogenic processes, primarily changing climate. At the base of the Monongahela Group, soils largely formed on proximal floodplains within early successional, fen, and clastic marsh ecosystems. The middle Monongahela, however, included well-developed paleosols formed on more stable, distal floodplains within dry woodland and brakeland ecosystems. In the upper Monongahela Group and the base of the Dunkard Group, soils continued to form on stable landscapes, but within fen and clastic marsh ecosystems. Higher in the Dunkard, soils included those forming on proximal floodplains, distal levees, and distal floodplains within brakeland ecosystems.

5.3.1 Influences of local-scale processes on landscapes and soil ecosystems

Local-scale processes greatly affect the type of soil formed as well as the distribution, orientation, and abundance of plants and animals (Schaetzl and Anderson 2005). The effects of these processes were recognizable in short-term vertical changes in pedotypes as well as lateral changes in contemporaneous paleosols. From the base of the Monongahela Group (S3P1) to midway up the Site 3 section (S3P7), autogenic processes were an important control on paleosol properties (Fig. 2). Many of the paleosols were immature and contained evidence of frequent disturbance or burial from flooding events (e.g., Kraus 1999; Buol et al. 2003). These paleosols also recorded shifts from well-drained to saturated conditions with minimal variation in grain size indicating quick changes local hydrology. These properties were likely caused by local-scale fluctuations in water table height due to changes in channel position or paleotopography (Kraus 1999; Retallack 2001; Counts and Hasiotis 2014). Rhizoliths and burrows were sparse and patchy, representing early colonizers with the ability to exploit bare sediment exposed for short amounts of time (Lavelle and Spain 2001; Retallack 2001).

Laterally contemporaneous profiles at the top of the Monongahela Group (sites 1 and 2) provided additional insight into autogenic processes influencing soil development. In the upper Monongahela Group both sites contained paleosols that likely formed in a fen (PT3) (Fig. 2). At site 1 this zone contained a limestone bed separating two paleosols (S1P1A, S1P1B) (Fig. 2). At site 2, however, the paleosol (S2P1) had no interbedded limestone unit. The limestone bed was interpreted as an isolated, overbank pond deposit resulting

from a localized depression or a locally elevated water table (Reading 1996). Additionally, the conglomerate truncating S1P1B at site 1 suggests high energy transport and a closer proximity to a paleochannel than site 2 (Fig. 2) (Reading 1996). An outcrop ~350 m east of site 1 also contains paleosols that formed in a fen at the top of the Monongahela Group (Hembree and Bowen 2017). However, a greater abundance of rhizoliths, burrows, preserved A horizons, and thicker paleosol profiles suggested a longer duration of stability than for the paleosols observed in this study (Hembree and Bowen 2017). These small-scale lateral changes along the same horizon are clear examples of autogenic controls such as topography and proximity to active channels, on soil development (Aslan and Autin 1998; Kraus 1999). A study of the Monongahela Group on outcrops ~30 km south of this study area classified upper Monongahela Group paleosols as Vertisols with better-drained soil conditions (Hembree and Carnes 2018). These large-scale differences were attributed to regional variation in topography; the localities of Hembree and Carnes (2018) were on the upper fluvial plain, whereas localities in this study were on the lower fluvial plain (e.g., Martin 1998).

For much of the studied Dunkard Group, contemporaneous paleosols between sites 1 and 2 were largely different. Above and below the paleosols were thick shales with mostly thin sandstones, suggesting changes from low to high energy representing shifts between overbank and channel environments (Fig. 2) (Reading 1996). This was different from the Hembree and Bowen (2017) locality where the same section consisted of mostly thick sandstones and thin shales indicating a greater influence of channel processes than in this study (Reading 1996).

5.3.2 Changes in climate and landscapes

Although local-scale processes controlled short-term changes in soil-forming conditions, regional-scale fluctuations in climate were the primary control on paleosol development through the study interval. Importantly, the paleosols revealed a climatic transition from the Late Pennsylvanian to Early Permian that was not gradual, but one that was erratic, with fluctuations in paleoprecipitation ranging from ~200 to 1400 mm/year. Paleosols indicative of both high and low MAP occurred throughout the studied section. As a result, the cluster analysis did not sort paleosols based on their stratigraphic position, landscape position, or soil ecosystem, but instead into three distinct groups based on climates with low, moderate, and high precipitation (Fig. 14).

At the base of the section (S3P1-S3P7), thicker (> 60 cm) paleosol profiles were the best indicators of climatic influence due to their longer duration of exposure and stability (e.g., Birkeland 1999; Kraus 1999; Retallack 2001). These paleosols were characterized by gleization features,

slickensides rare calcareous nodules, kaolinite, and smectite suggestive of a seasonally saturated environment (Sheldon and Tabor 2009). Estimated paleoprecipitation values for these profiles varied little and were relatively high (~1000–1300 mm/year) (Fig. 15). Overall, climate trended from wet to wet-dry and then back to wet with large-scale fluctuations in the middle. This interpretation agreed with contemporaneous western studies of Tabor and Montañez (2004) and DiMichele et al. (2006) who recognized redoximorphic features within the Late Pennsylvanian paleosols of north-central Texas suggesting higher precipitation for that interval.

Through the rest of the Monongahela Group (S3P8-S1P1B/S2P1) over-thickened and well-developed paleosol profiles represented longer periods of landscape stability on distal floodplains and showed a gradual upward decrease in paleoprecipitation values. These paleosols were interpreted to reflect dry and strongly seasonal conditions based on the occurrence of large-scale slickensides, carbonates nodules, absence of gleyed soil profiles, and abundant smectite (Retallack 2001; Buol et al. 2003; Sheldon and Tabor 2009). Paleoprecipitation estimates were stable and low ranging from ~200 to 700 mm/year. Paleosols studied by Hembree and Carnes (2018) 30 km to the south coeval to those near the top of this interval (S3P8-S3P9) had similarly low paleoprecipitation values (~800 mm/year) as did paleosols at the base of the neighboring Hembree and Bowen (2017) locality contemporaneous to S1P1A/B and S2P1 (~200 mm/year).

From the base to the middle of the studied Dunkard Group (S1P2/S2P2-S1P7/S2P4B), paleosols indicated wet to wet-dry, weakly seasonal conditions based on small slickensides, rare gleization features, and calcareous nodules (Retallack 2001; Buol et al. 2003). Paleoprecipitation estimates were high (~1300 mm/year) and stable except for a significant short-term decrease (~600–1100 mm/year) at S1P4/S2P4B. Vertical trends in paleoprecipitation between sites 1 and 2 were similar, even between dissimilar coeval paleosol profiles, supporting the paleoprecipitation estimates. Clay mineral data supported a transition to a wetter, less seasonal climate with kaolinite being the dominant clay mineral and smectite the least abundant (Sheldon and Tabor 2009). At the top of the Dunkard Group (S1P8), however, conditions shifted to a drier, more seasonal environment based on the presence of calcareous nodules, slickensides, absence of gleization features, and abundant smectite (Retallack 2001; Buol et al. 2003; Sheldon and Tabor 2009). Paleoprecipitation ranged from 600–800 mm/year and decreased up section. A decline in gleyed soil profiles from the Monongahela to Dunkard Group was recognized throughout this study area as well as the Hembree and Bowen (2017) locality supporting an overall upward drying trend. Similar studies conducted by Kessler et al. (2001), Mack et al. (2003), Giles et al. (2013), Counts and Hasiotis (2014), and Tanner and

Lucas (2017) in Kansas, New Mexico, and Oklahoma recognized an increase in seasonality and lowering MAP into the Permian using pedogenic properties. The co-occurrence of similar paleosol features at similar time intervals between this study and those in the midcontinent support climate as a primary control on soil development and landscape evolution at a regional scale during the Late Paleozoic.

6 Conclusion

A total of 40 measured paleosol profiles representing 11 pedotypes were identified in the Late Pennsylvanian to Early Permian Monongahela and Dunkard groups of southeastern Ohio. The main control on paleosol development was climate with small-scale variations attributed to local fluvial influences. Pedotypes 1, 2, 4, 6, and 11 were interpreted as Inceptisols that formed on proximal floodplains and distal levees within early successional vegetation and clastic marsh ecosystems with exposure times of 10^1 – 10^3 years. Pedotype 7 were well-developed Inceptisols with over-thickened profiles that formed on proximal to distal floodplains within clastic marsh and early successional vegetation ecosystems with exposure times of $\sim 10^3$ years. Pedotypes 5, 8, 9, and 10 consisted of highly developed Inceptisols or Vertisols with over-thickened profiles that formed on distal floodplains within early successional vegetation, brakeland, and dry woodland ecosystems with exposure times of 10^3 – 10^4 years. Pedotype 3 were well-developed Inceptisols that formed on distal floodplains in fen ecosystems with exposure times of 10^4 – 10^5 years.

Paleosol properties including gleization features provided evidence for an unstable, seasonally wet environment at the base of the Monongahela Group which represented the interval most affected by autogenic processes including channel-switching events. A transition to a more stable, seasonally dry environment then occurred through the rest of the Monongahela Group followed by seasonally wet conditions at the base to middle of the Lower Dunkard Group, with small scale fluctuations in between, before a switch to seasonally dry conditions at the top. These climatic trends generally agreed with local studies on correlative strata conducted by Hembree and Bowen (2017) and Hembree and Carnes (2018).

Allogenic processes were the major control on paleosol development throughout the studied section. This interpretation is supported by the grouping of paleosols based on paleoprecipitation values in the cluster diagram as well as other contemporaneous local and regional studies recognizing similar climatic trends in the data suggesting shifts in paleosol features through the section are not the result of local processes, but rather widespread regional climatic shifts. The climate trends in this study included several large

shifts in estimated paleoprecipitation values suggesting the onset of unstable climate conditions potentially related to the switch from interglacial to glacial states.

Acknowledgements We would like to thank the two anonymous reviewers for their helpful comments and suggestions to improve this paper. We would also like thank Drs. Gregory Nadon and Gregory Springer (Ohio University) for reviewing an earlier version of this manuscript as well as Jamie Halman, Zach Fernandes, and Thomas Johns for their help with the fieldwork. This project would not have been possible without funding by the American Chemical Society Petroleum Research Fund (52708-UR8) and the Ohio University Geological Sciences Graduate Student Alumni Grant.

Funding Funding for this research was provide by the American Chemical Society Petroleum Research Fund (52708-UR8) and the Ohio University Geological Sciences Graduate Student Alumni Grant.

Availability of data and material All data collected is available in the tables and appendices.

Compliance with ethical standards

Conflict of interest There is no conflict of interest or competing interests by either author.

Code availability Statistical analyses were performed using PAST version 3, free software available at <https://folk.uio.no/ohammer/past/>.

References

- Aslan, A., & Autin, W. J. (1998). Holocene flood-plain soil formation in the southern lower Mississippi valley: Implications for interpreting alluvial paleosols. *Geological Society of America Bulletin*, *110*, 433–449.
- Birkeland, P. W. (1999). *Soils and geomorphology*. New York: Oxford University Press.
- Blakey, R. C. (2008). Gondwana paleogeography from assembly to breakup—a 500 my odyssey. In C. R. Fielding, T. D. Frank, & J. L. Isbell (Eds.), *Resolving the Late Paleozoic ice age in time and space* (pp. 1–28). Boulder: Geological Society of America.
- Buatois, L., & Mángano, M. G. (2011). *Ichnology: Organism-substrate interactions in space and time*. Cambridge: Cambridge University Press.
- Buol, S. W., Southard, R. J., Graham, R. C., & McDaniel, P. A. (2003). *Soil genesis and classification* (5th ed.). Ames: Blackwell Publishing.
- Cecil, C. B. (2013). An overview and interpretation of the autocyclic and allocyclic processes and the accumulation of strata during the Pennsylvanian-Permian transition in the central Appalachian Basin, USA. *International Journal of Coal Geology*, *119*, 21–31.
- Cecil, C. B., Dulong, F. T., West, R. R., Stamm, R., Wardlaw, B., & Edgar, N. T. (2003). Climate controls on the stratigraphy of a Middle Pennsylvanian cyclothem in North America. In C. B. Cecil & N. T. Edgar (Eds.), *Climate controls on stratigraphy* (pp. 151–180). Tulsa: Society of Sedimentary Geology.
- Clendening, J. A. (1972). Stratigraphic placement of the Dunkard according to palynological assemblages. *Castanea*, *37*, 258–287.
- Counts, J. W., & Hasiotis, S. T. (2014). Distribution, paleoenvironmental implications, and stratigraphic architecture of paleosols

- in Lower Permian continental deposits of western Kansas, U.S.A. *Journal of Sedimentary Research*, 84, 144–167.
- D'Alessandro, A., & Bromley, R. G. (1987). Meniscate trace fossils and the *Muensteria-Taenidium* problem. *Paleontology*, 30, 743–763.
- DiMichele, W. A., Pfefferkorn, H. W., & Gastaldo, R. A. (2001). Response of Late Carboniferous and Early Permian plant communities to climate change. *Annual Review of Earth and Planetary Sciences*, 29, 461–487.
- DiMichele, W. A., Tabor, N. J., Chaney, D. S., & Nelson, J. W. (2006). From wetlands to wet spots: environmental tracking and the fate of Carboniferous elements in Early Permian tropical floras. In S. F. Greb & W. A. DiMichele (Eds.), *Wetlands through time* (pp. 223–248). Boulder: Geological Society of America.
- Driese, S. G., & Ober, E. G. (2005). Paleopedologic and paleohydrologic records of precipitation seasonality from Early Pennsylvanian “underclay” paleosols, USA. *Journal of Sedimentary Research*, 75, 997–1010.
- Eble, C. F., Greb, S. F., & Williams, D. A. (2001). The geology and palynology of Lower and Middle Pennsylvanian strata in the Western Kentucky Coal Field. *International Journal of Coal Geology*, 47, 189–206.
- Eble, C. F., Grady, W. C., & Blake, B. M. (2013). Dunkard Group coal beds: palynology, coal petrography and geochemistry. *International Journal of Coal Geology*, 119, 32–40.
- Fedoroko, N., & Skema, V. (2013). A review of the stratigraphy and the stratigraphic nomenclature of the Dunkard Group in West Virginia and Pennsylvania, USA. *International Journal of Coal Geology*, 119, 2–20.
- Fielding, C. R., Frank, T. D., & Isbell, J. L. (2008). The late Paleozoic ice age—a review of current understanding and synthesis of global climate patterns. In C. R. Fielding, T. D. Frank, & J. L. Isbell (Eds.), *Resolving the Late Paleozoic ice age in time and space* (pp. 343–354). Boulder: Geological Society of America.
- Gastaldo, R. A., DiMichele, W. A., & Pfefferkorn, H. W. (1996). Out of the icehouse into the greenhouse: A Late Paleozoic analog for modern global vegetational change. *GSA Today*, 6, 1–7.
- Genise, J. F., Mángano, M. G., Buatois, L. A., Laza, J., & Verde, M. (2000). Insect trace fossil associations in paleosols: The *Coprini-sphaera* ichnofacies. *Palaio*, 15, 33–48.
- Giles, J. M., Soreghan, M. J., Benison, K. C., Soreghan, G. S., & Hasiotis, S. T. (2013). Lakes, loess, and paleosols in the Permian Wellington Formation of Oklahoma, USA: Implications for paleoclimate and paleogeography of the Midcontinent. *Journal of Sedimentary Research*, 83, 825–846.
- Hasiotis, S. T. (2002). *Continental trace fossils*. Tulsa: Society for Sedimentary Geology.
- Hembree, D. I., & Blair, M. G. (2016). A paleopedological and ichnological approach to interpreting spatial and temporal variability in Early Permian fluvial deposits of the Lower Dunkard Group, West Virginia, USA. *Palaogeography, Palaeoclimatology, Palaeoecology*, 454, 246–266.
- Hembree, D. I., & Bowen, J. J. (2017). Paleosols and ichnofossils of the Upper Pennsylvanian-Lower Permian Monongahela and Dunkard groups (Ohio, USA): A multi-proxy approach to unraveling complex variability in ancient terrestrial landscapes. *Palaio*, 32, 295–320.
- Hembree, D. I., & Carnes, J. L. (2018). Response of soils and soil ecosystems to the Pennsylvanian-Permian climatic transition in the upper fluvial plain of the Dunkard Basin, southeastern Ohio, USA. *Geosciences*, 8, 1–35.
- Hembree, D. I., & Nadon, G. C. (2011). A paleopedologic and ichnologic perspective of the terrestrial Pennsylvanian landscape in the distal Appalachian Basin, USA. *Palaogeography, Palaeoclimatology, Palaeoecology*, 312, 138–166.
- Kessler, L. P., Soreghan, G. S., & Wacker, H. J. (2001). Equatorial aridity in western Pangea: Lower Permian loessite and dolomitic paleosols in northeastern New Mexico, USA. *Journal of Sedimentary Research*, 71, 817–832.
- Kimmins, J. P. (1997). *Forest ecology*. New Jersey: Prentice-Hall.
- King, R. M. (2008). *Fluvial architecture of the interval spanning the Pittsburgh and Fishpot Limestones (Late Pennsylvanian), southeastern Ohio, USA Master's Thesis*. Athens: Ohio University.
- Kiviat, E. (2010). *Phragmites management sourcebook for the Tidal Hudson River and the northeastern states*. Annandale: Hudsonia Ltd.
- Kraus, M. J. (1999). Paleosols in clastic sedimentary rocks: their geologic applications. *Earth-Science Reviews*, 47, 41–70.
- Kraus, M. J., & Hasiotis, S. T. (2006). Significance of different modes of rhizolith preservation to interpreting paleoenvironmental and paleohydrologic settings: examples from Paleogene paleosols, Bighorn Basin, Wyoming, USA. *Journal of Sedimentary Research*, 76, 633–646.
- Lavelle, P., & Spain, A. V. (2001). *Soil ecology*. Dordrecht: Kluwer Academic Publishers.
- Lucas, S. G. (2013). Vertebrate biostratigraphy and biochronology of the upper Paleozoic Dunkard Group, Pennsylvania-West Virginia-Ohio, USA. *Journal of Coal Geology*, 119, 79–87.
- Mack, G. H., James, W. C., & Monger, H. C. (1993). Classification of paleosols. *Geological Society of America Bulletin*, 105, 129–139.
- Mack, G. H., Leeder, M., Perez-Arlucea, M., & Bailey, B. D. J. (2003). Early Permian silt-bed fluvial sedimentation in the Orogrande basin of the ancestral Rocky Mountains, New Mexico, USA. *Sedimentary Geology*, 160, 159–178.
- Mack, G. H., Tabor, N. J., & Zollinger, H. J. (2010). Paleosols and sequence stratigraphy of the Lower Permian Abo Member, south-central New Mexico, USA. *Sedimentology*, 57, 1566–1583.
- Marriott, S. B., & Wright, V. P. (1993). Paleosols as indicators of geomorphic stability in two Old Red Sandstone alluvial suites, South Wales. *Journal of the Geological Society of London*, 150, 1109–1120.
- Martin, W. D. (1998). Geology of the Dunkard Group (Upper Pennsylvanian-Lower Permian) in Ohio, West Virginia, and Pennsylvania. Ohio Department of Natural Resources. *Division of Geological Survey*, 73, 1–49.
- Mikaš, P., & Uchman, A. (2013). Beetle burrows with a terminal chamber: A contribution to the knowledge of the trace fossil *Macanopsis* in continental sediments. *Palaio*, 28, 403–413.
- Montañez, I. P., & Cecil, C. B. (2013). Paleoenvironmental clues archived in non-marine Pennsylvanian-Lower Permian limestones of the central Appalachian Basin, USA. *International Journal of Coal Geology*, 119, 41–55.
- Montañez, I. P., & Poulsen, C. J. (2013). The Late Paleozoic ice age: An evolving paradigm. *Annual Review of Earth and Planetary Sciences*, 41, 629–656.
- Motzkin, G. (1994). Calcareous fens of western New England and adjacent New York State. *Rhodora*, 96, 44–68.
- Nordt, L., & Driese, S. (2010). New weathering index improves paleorainfall estimates from Vertisols. *Geology*, 38, 407–410.
- Pfefferkorn, H. W., & Wang, J. (2009). *Stigmariopsis*, *Stigmaria asiatica*, and the survival of the *Sigillaria brardii-ichthyolepis* group in the tropics of Late Pennsylvanian and Early Permian. *Palaeworld*, 18, 130–135.
- PiPujol, M. D., & Buurman, P. (1994). The distinction between ground-water gley and surface-water gley phenomena in Tertiary paleosols of the Ebro basin, NE Spain. *Palaogeography, Palaeoclimatology, Palaeoecology*, 110, 103–113.
- Reading, H. G. (1996). *Sedimentary environments: Processes, facies, and stratigraphy*. Oxford: Blackwell Science.
- Retallack, G. J. (2001). *Soils of the past: an introduction to paleopedology*. Oxford: Blackwell Science.
- Schaetzl, R. J., & Anderson, S. (2005). *Soils: Genesis and geomorphology*. Cambridge: Cambridge University Press.

- Schneider, R. J., Lucas, S. G., & Barrick, J. E. (2013). The Early Permian age of the Dunkard Group, Appalachian basin, U.S.A., based on spiloblatinid insect biostratigraphy. *International Journal of Coal Geology*, *119*, 88–92.
- Sheldon, N. D., & Tabor, N. J. (2009). Quantitative paleoenvironmental and paleoclimatic reconstruction using paleosols. *Earth-Science Reviews*, *95*, 1–52.
- Smith, J. J., & Hasiotis, S. T. (2008). Traces and burrowing behaviors of the cicada nymph *Cicadetta calliope*: neoichnology and paleoecological significance of extant soil-dwelling insects. *Palaaios*, *23*, 503–513.
- Smith, J. J., Hasiotis, S. T., Kraus, M. J., & Woody, D. T. (2008). *Naktodemasis bowni*: New ichnogenus and ichnospecies for adhesive meniscate burrows (AMB), and paleoenvironmental implications, Paleogene Willwood Formation, Bighorn basin, Wyoming. *Journal of Paleontology*, *82*, 267–278.
- Soil Survey Staff. (2014). *Keys to taxonomy* (12th ed.). Washington D.C.: U.S. Government Printing Office.
- Sturgeon, M. T. (1958). The geology and mineral resources of Athens County, Ohio. *Ohio Division of Geological Survey Bulletin*, *57*, 1–600.
- Tabor, N. J., & Montañez, I. P. (2004). Morphology and distribution of fossil soils in the Permo-Pennsylvanian Wichita and Bowie Groups, north-central Texas, USA: Implications for western equatorial Pangean palaeoclimate during icehouse–greenhouse transition. *Sedimentology*, *51*, 851–883.
- Tabor, N. J., & Poulsen, C. J. (2008). Paleoclimate across the Late Pennsylvanian–Early Permian tropical palaeolatitudes: A review of climate indicators, their distribution, and relation to palaeo-physiographic climate factors. *Palaeogeography, Palaeoclimatology, Palaeoecology*, *268*, 293–310.
- Tanner, L. H., & Lucas, S. G. (2017). Paleosols of the Upper Paleozoic Sangre de Cristo Formation, north-central New Mexico: Record of Early Permian paleoclimate in tropical Pangea. *Journal of Paleogeography*, *6*, 144–161.
- Trendall, A. M., Nordt, L. C., Atchley, S. C., Leblanc, S. L., & Dworkin, S. I. (2013). Determining floodplain plant distributions and populations using paleopedology and fossil root traces: Upper Triassic Sonsela Member of the Chinle Formation at Petrified Forest National Park, Arizona. *Palaaios*, *28*, 471–490.
- Wright, V. P., Taylor, K. G., & Beck, V. H. (2000). The paleohydrology of Lower Cretaceous seasonal wetlands, Isle of Wight, Southern England. *Journal of Sedimentary Research*, *70*, 619–632.

Publisher's Note Springer Nature remains neutral with regard to jurisdictional claims in published maps and institutional affiliations.